

Progress and Strategies of MOFs in Catalyzing Conversion Processes in Lithium-Sulfur Batteries

Yaru Wang,^[a] Xingyou Rao,^[a] Zhengdao Pan,^[a] Yan Zhao,^[a] Yalong Zheng,^[a] Yichao Luo,^[a] Xinyu Jiang,^[a] Yutong Wu,^[a] Xiang Liu,^[a] Zhoulu Wang,^{*[a]} and Yi Zhang^{*[a]}

Lithium-sulfur (Li–S) batteries have attracted considerable attention due to their advantages, such as high specific capacity, high energy density, environmental friendliness, and low cost. However, the severe capacity fading caused by shuttle effect of polysulfide needs to be addressed before the practical application of Li–S batteries. Crystalline porous materials including MOFs have generated great interest in energy storage fields especially batteries, because the ordered porous frameworks can offer a fast-ionic transportation. Nevertheless, the intrinsic low conductivity of MOFs limits their rapid development in lithium-sulfur batteries. This review mainly discusses the latest research progress on MOF main materials in Li–S batteries. The working principle of Li–S batteries and the classical “adsorption-catalysis-conversion” strategy are briefly introduced. Specifically, three modification methods (non-metal

atom doping, single-atom, and dual-atom doping modifications) applied in MOF-based materials are analyzed and summarized, along with their respective mechanisms and advantages and disadvantages. Ligand doping is an effective strategy that can regulate the structure and properties of MOFs, thereby enhancing their catalytic activity and adsorption capacity towards polysulfides. Through ligand doping, key parameters such as the pore size, surface charge, and active site density of MOFs can be controlled, thereby influencing the adsorption and conversion of polysulfides on MOFs surfaces. Furthermore, crucial insights for the rational design of advanced MOF-based materials for lithium-sulfur batteries and the exploration of the main challenges and future directions for their application were also discussed.

1. Introduction

Rapidly depleting fossil fuel resources coupled with increasing environmental pollution has accelerated the pace of developing environmentally sustainable and high-energy-density renewable energy.^[1,2] Replacing fossil fuels with clean energy is of significance in creating crucial environmental, social and economic benefits for a more sustainable future. Currently, the rechargeable batteries on the market do not fully satisfy the fast-growing global energy demand, and the “range anxiety” continues to be a major concern, particularly for their application in electric vehicles (EVs).^[3–5] Developing battery systems with higher sustainability to store the intermittent renewable energy is critical to fulfill the promise of reducing carbon footprints and addressing climate change.^[6–10] Lithium-sulfur (Li–S) chemistry is a promising choice for next-generation rechargeable batteries due to its high theoretical specific capacity, cost advantage, and environmental friendliness.^[11–13] In addition, sulfur has the advantages of low cost, abundant reserves, and clean friendliness.^[14] Therefore, Li–S batteries are considered to be one of the most promising next-generation energy storage devices for LIB.^[15] Despite all these merits, Li–S batteries have undergone a tortuous developing road and

multiple intrinsic drawbacks need to be addressed before their practical application.^[16] These obstacles include: 1) the practical application of Li–S battery is still hampered by the insulation of the active material and discharge products;^[17–19] 2) The Li dendrite growth induced by the nonuniformity Li deposition and the passivation layer formed by chemical reactions between active LiPSs and fresh Li would lead to the rapid decay of batteries and potential safety hazard^[20–22]; 3) The high volume expansion ($\approx 80\%$) of solid sulfur into Li_2S exerts heavy stress on the host structure and causes the detachment of sulfur species from the conductive substrate^[23]; and 4) The notorious shuttle effect caused by soluble lithium polysulfides (LiPSs) results in the loss of active materials and rapid capacity decrease.^[24]

In the past decade, numerous efforts have been devoted to overcome these above-mentioned challenges.^[25–29] Table 1 summarizes the issues with lithium-sulfur batteries, corresponding strategies, and mechanisms for improvement. Among them, the shuttle effect is the main reason for the irreversible loss of active substances, the attenuation of battery life, and the low coulombic efficiency of lithium-sulfur batteries, so inhibiting the shuttle effect is one of the key ways to improve the electrochemical performance of lithium-sulfur batteries.^[30] At present, the basic research on the inhibition of shuttle effect is mainly carried out from three aspects: 1) Physical limitations: including reducing or eliminating the solubility of lithium polysulfide in the electrolyte and inhibiting the shuttle effect from the source, setting up obstacles between the positive electrode and the electrolyte to cut off the migration path of lithium polysulfide to the negative electrode, modifying the surface of lithium

[a] Y. Wang,[†] X. Rao,[†] Z. Pan, Y. Zhao, Y. Zheng, Y. Luo, X. Jiang, Y. Wu, X. Liu, Z. Wang, Y. Zhang
School of Energy Sciences and Engineering, Nanjing Tech University, Nanjing, Jiangsu Province 211816, China
E-mail: 1zlwang@njtech.edu.cn
2zhanyang@njtech.edu.cn

Table 1. Issues with Li–S batteries, corresponding strategies and improvement mechanisms.

Existing Issues	Corresponding strategies	Improvement mechanisms
The active material sulfur is insulating	<ol style="list-style-type: none"> Adding conductive additives to the sulfur cathode^[42] Combine sulfur with conductive materials (like carbon materials) or conductive polymers (like polyaniline, polypyrrole, etc.) to create sulfur-based composites^[43] Modifying sulfur electrodes with functionalized conductive polymers (like polymer electrolytes)^[44] Using highly conductive electrolytes or modified electrolytes (like solid electrolytes or functionalized liquid electrolytes)^[45] 	<ol style="list-style-type: none"> By providing an electronic conductive pathway, the insulating effect of sulfur is reduced, which improves the efficiency of electron conduction The composite materials not only enhance the conductivity of sulfur but also provide extra mechanical support to prevent electrode cracking due to the expansion and contraction of sulfur Functional conductive polymers can enhance electronic conductivity and improve the interface contact with sulfur, thereby reducing the insulating effect of sulfur Highly conductive electrolytes can reduce the dissolution of polysulfides, thereby minimizing the shuttle effect while also enhancing the overall conductivity and stability of the battery
Lithium dendrite growth	<ol style="list-style-type: none"> Use an electrolyte with high ionic conductivity or develop a solid-state electrolyte^[46] Add dendrite inhibitors, like nanoparticles and ionic liquids, to the electrolyte^[47] Introduce three-dimensional conductive scaffold materials in the anode, such as carbon nanotube arrays and conductive polymer networks^[48] 	<ol style="list-style-type: none"> High ionic conductivity electrolytes can boost the conduction efficiency of lithium ions, reduce the interfacial impedance between the electrolyte and the lithium metal surface, thereby lowering the localized current density and decreasing the formation of dendrites Dendrite inhibitors can form a protective layer on the lithium metal surface, change the deposition pattern of lithium ions, and reduce the growth of dendrites A three-dimensional conductive framework can provide an even distribution of current and more space for Li^+ storage, reducing local current density, improving the uniformity of lithium deposition, and preventing the formation of dendrites
Volume expansion during the conversion of solid sulfur to Li_2S	<ol style="list-style-type: none"> Introduce elastic materials or 3D conductive frameworks, like carbon nanotubes, graphene, or conductive polymers, into sulfur cathodes^[49] Adjust the design of sulfur electrodes, like optimizing the thickness, porosity, or using composite materials^[50] A protective layer, like a polymer or oxide film, is coated on the surface of the sulfur cathode^[51] 	<ol style="list-style-type: none"> Elastic materials or frameworks can provide support and cushioning, absorbing the stress caused by volume expansion The right porosity and structural design can allow for more expansion and contraction of sulfur without damaging the overall structure of the electrode The protective film can buffer the mechanical stress caused by volume changes and prevent direct contact between the sulfur material and the electrolyte, thereby reducing material shedding and performance degradation
Shuttle effect of LiPSs	<ol style="list-style-type: none"> Physical limitations: Using porous carbon materials as electrode supports; Adding conductive carbon materials to the sulfur cathode Chemical adsorption: Using polar groups to form bonds or adsorption (for example, the heteroatomic oxygen and sulfur in the conductive polymer PEDOT have strong coordination interactions with lithium atoms in Li_2S; some transition metal compounds (such as MnO_2, SnO_{2n-1}, etc.) can form chemical adsorption or catalytic reactions during thermal treatment or electrochemical processes^[31]) Catalytic conversion: Transition metal compounds^[52], conductive polymer doping^[53], and metal-sulfide composites^[54] 	<ol style="list-style-type: none"> The material's porous structure can capture and restrict the migration of polysulfides; Conductive materials can enhance the conductivity of sulfur and restrict the diffusion of polysulfides through physical barriers Polar groups (such as carboxyl, amino, or hydroxyl groups) can form chemical bonds with sulfur atoms or lithium atoms in polysulfides. This chemical bonding can effectively capture and stabilize polysulfides, and can also interact with polysulfides through physical adsorption; Transition metal compounds can promote the reduction or oxidation reactions of polysulfides, thereby altering the properties and behavior of polysulfides and reducing the shuttle effect Transition metal compounds provide additional active sites and lower the energy barrier of reactions, accelerating the reduction of polysulfides; Conductive polymers not only provide conductive pathways but also have chemical adsorption capabilities for polysulfides; Metal sulfides, with their strong interactions with sulfur atoms, can promote the electrochemical conversion reactions of polysulfides

polysulfide and isolating the contact reaction between lithium polysulfide and lithium metal; 2) Chemical adsorption: using polar groups to form bonds or adsorption (such as the heteroatomic oxygen and sulfur in the conductive polymer PEDOT and the lithium atoms in Li_2S have strong coordination chelation); surface nitrogen doping of matrix carbon materials can also effectively improve the chemical adsorption between sulfur and oxygen-containing functional groups; and some

transition metal compounds (such as MnO_2 , TiO_{2n-1} , etc.) in the process of heat treatment or electrochemical reaction, bonding or catalysis between sulfur and indirect formation of chemical adsorption^[31]; 3) Catalytic conversion: a variety of functional materials (such as transition metal compounds, single-atom catalysts, small organic molecules, metal-organic framework materials, MOFs, etc.) are widely used in the adsorption and catalytic conversion of LiPSs, but traditional metal compounds

usually lack sufficient active sites. Compared with traditional metal compounds, single-atom catalysts have more active sites and high catalytic activity, but their mass activity or volumetric activity is often low, which largely limits the practical application of single-atom catalysts.^[32] The catalytic activity of organic small molecules is high, but their dissolution and diffusion in the electrolyte may lead to the weakening of the catalytic effect and the rapid decay of battery capacity. However, MOFs could theoretically overcome the shortcomings of traditional catalysts by modulating functional sites for the adsorption and catalysis of LiPSs at the molecular level.^[33] As a significant new type of porous materials besides zeolites and carbon nanotubes, MOFs have attracted extensive attention in the field of electrochemistry over past two decades.^[34–40] At present, the active site of MOFs is relatively single and its insulation is not conducive to high catalytic efficiency, so the development of conductive MOFs catalysts with high-density adsorption sites and multiple catalytic sites may achieve more efficient LiPSs catalytic conversion efficiency.^[41] Therefore, this paper focuses on summarizing the recent applications of MOFs-based materials, primarily through doping and modification, for the multi-step catalytic conversion of lithium polysulfides in lithium-sulfur batteries. Non-metal doping can improve the material's electronic structure, enhance its catalytic performance, or increase its stability. Single-metal doping involves introducing a single metal element into the MOF framework to adjust its physicochemical properties. Finally, dual-metal doping involves incorporating two different metal ions into the MOFs simultaneously. This method can combine the advantages of both metals to optimize catalytic performance. By adjusting the ratio and distribution of the dual metals, the functionality and applicability of MOFs can be further enhanced. Research into these doping modification techniques is crucial for improving the performance and practical applications of MOFs. Finally, the main challenges and future prospects of MOFs-based catalysts for actual LSBs are proposed.

2. Lithium-Sulfur Battery Conversion Catalysis Mechanism

Classically, Li–S batteries are composed of sulfur composite cathode, electrolyte, separator and metallic lithium anode. When discharged, lithium metal anode generates electrons and Li^+ ions, and then the Li^+ ions diffuse toward cathode side through electrolyte. Meanwhile, electrons travel from the external circuit to sulfur molecular in cathode, and the elemental sulfur will be reduced to lithium polysulfides. When charged, Li^+ ions move toward the anode side and will be reduced to elemental lithium after accepting electrons provided by external electric source.^[55,56] At the same time, lithium sulfide is oxidized to elemental sulfur by losing electrons. However, the molecular structure of sulfur is a cyclic ring composed with eight sulfur atoms (S_8), the bonds in S_8 ring can be dissociated and reconstructed in many ways which will induce complicated redox reaction mechanism.^[57,58] The reduction reaction (SRR) of S during the discharge of lithium-sulfur batteries involves a complex multi-step conversion process of 8 electrons from the S_8 molecule to the Li_2S solid. As shown in Figure 1a, the S_8 molecule first forms a long chain of Li_2S_8 with lithium ions in the voltage range of 2.7–2.4 V, followed by successive cleavage of S–S bonds, then forms Li_2S_6 or Li_2S_4 in the range of 2.3–2.1 V, and finally transforms into insoluble Li_2S_2 and Li_2S at 2.1–1.7 V.^[59] SRR boils down to two stages: solid-liquid reduction from sulfur to polysulfide and Li_2S deposition. The former presents a relatively easy transformation process, while the latter needs to overcome high energy barriers, resulting in slow dynamics. Therefore, the Li_2S deposition process can be considered as a rate-determining step for the entire SRR.^[60] Improving the redox kinetics of SRR and lowering the energy barrier will significantly alleviate the shuttle effect and increase the output potential of the battery. In the Li_2S system, catalysis mainly includes the following processes: adsorption of soluble LiPSs, diffusion of adsorbed LiPSs, and interconversion between LiPSs and Li_2S .^[61] Effective LiPSs adsorption is a prerequisite for subsequent catalytic conversion, and the required catalytic materials should be balanced between the above adsorption

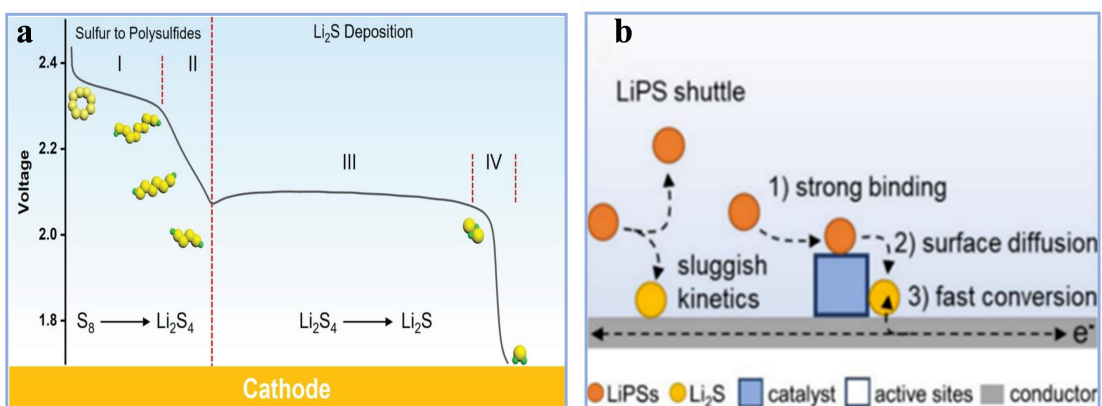


Figure 1. (a) Schematic illustration of a typical charge-discharge profile of a Li–S battery, including four stages^[60]; (b) Illustration of the catalytic mechanism in LSBs.^[62]

and catalysis to achieve a smooth “LiPSs adsorption-diffusion-conversion” process (Figure 1b).^[62]

3. Applications and Advantages of MOFs in Lithium-Sulfur Batteries

3.1. Practical Applications of MOFs in Lithium-Sulfur Batteries

MOFs are a class of porous materials with periodic network structure formed by the self-assembly of inorganic metal ions (or metal ion clusters) and organic ligands through coordination, and these MOFs contain a large number of chemically active sites (such as Lewis acid-base pairs or functionalized organic functional groups) that can have an affinity for polysulfides and active substances sulfur.^[63] The Huang team proposed a universal multimodal strategy for the development of a series of multi-site catalytic metal-organic frameworks (MSC-MOFs). Theoretical calculations indicate that within the nanocages of MSC-MOFs, polar functional groups ($-\text{NH}_2$) and exposed mixed-valence metal sites form collaborative adsorption/catalytic interfaces. This provides new insights for the design and application of advanced porous catalytic materials.^[64] Moreover, due to their strong functionality, high porosity, large specific surface area, tunable pore size, biomimetic catalysis, and good biocompatibility, MOF-based materials show significant improvements in molecular and ionic sieving capabilities. Additionally, they can effectively capture and support the transport of lithium ions, increase the conductivity of the electrodes, and thus contribute to enhancing the overall electrochemical performance of lithium-sulfur batteries.^[65]

ZIF-8, ZIF-67, and MOF-5 are three important and widely used MOF materials in lithium-sulfur batteries, and their anchoring effect on polysulfides has significant implications for the development of other MOF materials. Wu et al.^[66] investigated the adsorption of reactant S_8 , LiPSs intermediates, and product Li_2S on these three MOFs. The theoretical calculations indicate that the adsorption of S_8 occurs through electrostatic interactions; the adsorption of LiPSs intermediates is facilitated by Li-heteroatom (N/O) bonding; and the Li-heteroatom bonding remains present for the adsorption of product Li_2S . Additionally, metal center (Zn/Co)-S bonding exists in ZIF-8 and ZIF-67, which further enhances the adsorption effect. This reveals the roles of metal centers and organic ligands in the

anchoring effect. Additionally, due to their highly tunable porous structure, MOFs can optimize the interfacial reactions between the electrolyte and the electrode materials. This interfacial adjustment helps to reduce interfacial impedance and enhance the power performance of the battery. Furthermore, the flexible structure of MOFs can alleviate the volume expansion of electrode materials during lithium plating, thus improving the cycling life of the battery. Table 2 summarizes the practical applications of MOFs in lithium-sulfur batteries at various rates, as well as the mechanisms of action.

In conclusion, MOFs demonstrate unique advantages in their application in lithium-sulfur batteries, which will provide them with broader prospects in the field of high-energy-density energy storage.

3.2. Stability and Sustainability of MOFs

Li-S batteries are widely regarded for their high energy density and potential low cost. However, the stability and sustainability of their materials are crucial for commercialization. Firstly, sulfur generates soluble polysulfides during charge and discharge cycles, which can cause capacity fade and impact cycle life. To ensure battery stability, efficient electrolytes and protective membranes are needed to control the dissolution and migration of polysulfides. Secondly, the sustainability of lithium-sulfur batteries involves the environmental impact of materials and resource scarcity. Choosing eco-friendly materials and optimizing recycling processes can reduce dependence on rare resources and lower environmental impact. Therefore, enhancing the material stability and sustainability of lithium-sulfur batteries is essential for their future widespread application.

The highly ordered porous structure of MOFs can effectively accommodate sulfur while maintaining structural integrity. During charge and discharge cycles, the volume change of sulfur can induce stress and cracking in the electrode materials. The framework structure of MOFs can effectively alleviate these stresses and reduce electrode degradation, thereby enhancing the cycling stability of the battery. Additionally, MOFs’ structures can be further improved through post-processing or functionalization to enhance overall battery stability, with some MOFs showing good structural stability under high voltage or high temperatures, greatly improving the safety and long-term stability of lithium-sulfur batteries. Moreover, the application of MOFs in lithium-sulfur batteries also highlights their superior sustainability. MOFs can be produced through green synthesis

Table 2. Practical applications of MOFs in Lithium-Sulfur Batteries at various rates and their mechanisms of action.

Applications	Mechanisms	Reference
Provide sites for catalysis	Lewis acid-base pairs or functionalized organic groups interact with polysulfides	[63,64]
Increase electrode conductivity	High porosity structure accelerates Li^+ transport	[65]
Polysulfide adsorption	S_8 : electrostatic adsorption; LiPSs/ Li_2S : Li bonds with heteroatoms	[66]
Inhibitory shuttle effect	The high specific surface area and porous structure can effectively capture and stabilize dissolved polysulfides	[67]

methods and typically use abundant metal ions and organic ligands, which consume fewer resources. After the battery's life ends, MOFs can be regenerated and recycled through physical or chemical methods, reducing the need for new materials and environmental pollution. Thus, this review will discuss the application of MOFs in lithium-sulfur batteries, focusing on the catalytic conversion mechanisms of polysulfides through MOF doping and modification.

4. The Strategies of MOF Catalytic Conversion in Lithium-Sulfur Batteries

In recent years, there has been significant advancement in the deep study of adsorption and catalytic synergistic effects on polysulfides in lithium-sulfur batteries, with further improvements in the design and optimization of modification methods. On one hand, complex heterogeneous structures are designed to increase the electrode's surface area and active sites, enhancing the adsorption capacity and electron transfer rate of polysulfides, thereby suppressing their dissolution and shuttle effects. For instance, Zhu et al.^[68] developed a novel VC-VO heterostructure (VC-VO/HPC) supported on hierarchical porous carbon matrices. The VC-VO heteroparticles interact with polysulfides, evolving into V_5S_8 on their surfaces. This accelerates overall electron transfer rates and facilitates the conversion between sulfur species. As a result, it achieves efficient anchoring, rapid diffusion, and effective conversion of LiPSs simultaneously. In lithium-sulfur batteries, metallic manganese can not only serve as an effective polysulfide adsorbent but also provide additional electronic conductive pathways, facilitating electron transport and ion diffusion. Phosphides can act as conductive additives or catalysts, playing an important role in inhibiting the dissolution of polysulfides and the shuttle effect. Therefore, Zhu's team synthesized MnP-Mn₂P nanoparticles through a one-pot thermal treatment, which were uniformly dispersed on porous carbon and utilized as the sulfur host (MnP-Mn₂P/C@S) for lithium-sulfur batteries. In cycling tests at 5 C over 2000 cycles, the capacity decay rate per cycle was only 0.013%, providing a certain theoretical support for the practical application of lithium-sulfur batteries.^[69] Besides the research on manganese phosphide heterostructures (MnP-Mn₂P/C), recently, the team developed MnP-MnO₂ heterostructure catalysts via a one-step heat treatment method. Through a series of in-situ characterizations and theoretical calculations, it was confirmed that during charge and discharge processes, the MnP-MnO₂ heterostructure undergoes surface sulfidation to form the MnS₂ phase. This significantly accelerates the sulfur reduction reaction (SRR) and Li₂S activation, effectively inhibiting the shuttling of lithium polysulfides (LiPSs) and facilitating their catalytic conversion.^[70] In addition to exploring manganese phosphides, further validation was conducted on the adsorption and catalytic effects of niobium phosphide towards polysulfides. Due to its excellent electrical conductivity, acting as a sulfur activation agent, and effective inhibition of dendrite growth, the niobium phosphide-niobium carbide heterostruc-

ture dispersed on porous carbon (NbP-NbC/C) demonstrated efficient adsorption and catalysis of polysulfides.^[71] In conclusion, heterogeneous structures can effectively adsorb and catalytically convert LiPSs, but their complex preparation process makes precise structural control challenging, potentially leading to instability that affects battery cycling stability. Metal-organic frameworks (MOFs), with tunable pore structures and abundant active sites, offer more precise control over the adsorption and catalytic reaction processes of polysulfides. They are considered promising candidates as excellent electrocatalysts for lithium-sulfur batteries. Therefore, this article will summarize the use of MOFs, primarily through doping and modification, to explore their bidirectional synergistic adsorption-catalysis effect on LiPSs.

Studies have shown that the electrocatalytic process of many catalytic materials can help accelerate the conversion kinetics of polysulfides, reduce the accumulation of polysulfides, and inhibit the shuttle effect, and a variety of electrocatalysts have shown great effects in improving battery performance.^[72] In recent years, MOFs have proven to be very promising catalysts in the field of catalysis. In the past few years, the application of MOFs in the field of electrochemical energy storage has attracted more and more attention due to its high catalytic activity due to its abundant organic linker groups and metal active centers. A series of MOFs-based catalytic materials with excellent LiPSs adsorption and catalytic activities were constructed through selective ligand doping strategies to achieve high-performance lithium-sulfur batteries. In this paper, we summarize the research progress of MOFs in the field of LSB catalytic conversion in recent years according to the categories of non-metal doping, single metal doping and bimetal doping as carriers.

4.1. Non-Metallic Doped MOF

Although MOFs can provide abundant polar catalytic sites to accelerate the redox reaction kinetics of lithium polysulfide and inhibit the shuttle effect, they have a great impact on the kinetic performance of sulfur cathode due to their inherent poor conductivity. Therefore, combining MOFs with materials with good conductivity is one of the main ways to improve conductivity and optimize battery performance.

Carbon material, with good conductivity, high porosity, strong adsorption capacity, low cost and other advantages.^[73] The use of carbon materials to form a conductive network to make up for the insulation defects of sulfur element, the use of carbon materials porosity, so that the sulfur can be evenly distributed in the carbon material gap, so as to increase the load of sulfur, and the abundant voids also provide more active sites, which can physically limit the position of polysulfides, and prevent the dissolution and diffusion of polysulfides, and inhibit the "shuttle effect".^[74] For example, He and coworkers developed a new integrated interlayer-current collector based on thiol-containing MOF-decorated carbon cloth (CC@UiO-66(SH)₂) for advanced Li-S batteries.^[75] This two-in-one integrated architecture endows the sulfur cathode with fast electron/ion transport

and efficient chemical confinement of polysulfides. For CC@UiO-66(SH)₂, the surfaces of the smooth carbon fibers of pure CC are uniformly covered with UiO-66(SH)₂ nanoparticles, making them rough, which provides more sites for bonding with polysulfides.^[76] The mechanism of CC@UiO-66(SH)₂ inhibiting polysulfide shuttling is proposed in Figure 2a. On the one hand, the *in situ*-grown UiO-66(SH)₂ shares the electron/ion transport pathway with CC; therefore, CC@UiO-66(SH)₂ with the conductive network can work as an effective current collector to reserve active materials and improve sulfur utilization. Meanwhile, the abundant thiol groups in UiO-66(SH)₂ can act as active sites to capture polysulfides by lithium bonding and covalent interactions. On the other hand, UiO-66(SH)₂ acts as an interlayer to further anchor polysulfides and reuse them. Therefore, the Li-S batteries with this integrated interlayer-current collector result in excellent electrochemical performances.^[77] In recent years, it has been found that the Li⁺ solvation structure can form special ion transport channels by adjusting the solvation sheath involving external anions, promoting Li⁺ movement and significantly influencing Li⁺ kinetics.^[78–80] Liu et al.^[81] designed a bridging MOF-carbon interface to catalytically accelerate the process of lithium-ion desolvation and polysulfide conversion by using metal-organic framework materials with functional groups. The C–N bridged bond in MOF@CC structures are constructed by “welding” highly conductive carbon layer and MOF particles together (Figure 2b), providing the pathway of electronic exchange for

high catalytic efficiency. Consequently, although there are some polysulfides shuttles into electrolyte, it will be trapped by MOF@CC and takes electrochemical reaction with the bare Li⁺ from Li⁺-solvent complex under the assistance of electrons from the C–N bridge between MOF and carbon. The increase in σ and t_{Li⁺}⁺ of MOF@CC@PP may be due to the unique MOF@PP modification layer. When the Li⁺-solvent complexes pass through the PP membrane, because these complicated complexes require additional energy to remove the solvent molecules to obtain the Li⁺ ions, this will form a larger barrier and consume a larger energy barrier (Figure 2c). On the contrary, when the Li⁺-solvent complex passes through the narrow channel of MOF@CC layer, the outer solvated sheath can be screened out, and the active C–N bridge bond in the MOF@CC structure serves as the catalytic site, which can accelerate the Li⁺ de-solvatization in the complicated complexes. Participate in the Redox reaction of polysulfides without consuming too much energy and accelerate the reaction kinetics (Figure 2d). As exhibited in Figure 2e, the precipitation capacity of Li₂S in MOF@CC@PP system is 646 mAh g⁻¹, which is the highest among all these three systems (499 mAh g⁻¹ in MOF+CC@PP, 183 mAh g⁻¹ in PP system). A higher Li₂S precipitation capacity and earlier current response well indicate a faster transformation rate from polysulfides to Li₂S.^[82] Moreover, the CV curves in Figure 2f show a higher redox current and a smaller battery polarization in MOF@CC@PP, again proving its excellent conversion performance.^[83] In addition, as shown in Figure 2g, the cycle performance of the large-area bag battery can also remain stable under the condition of lean

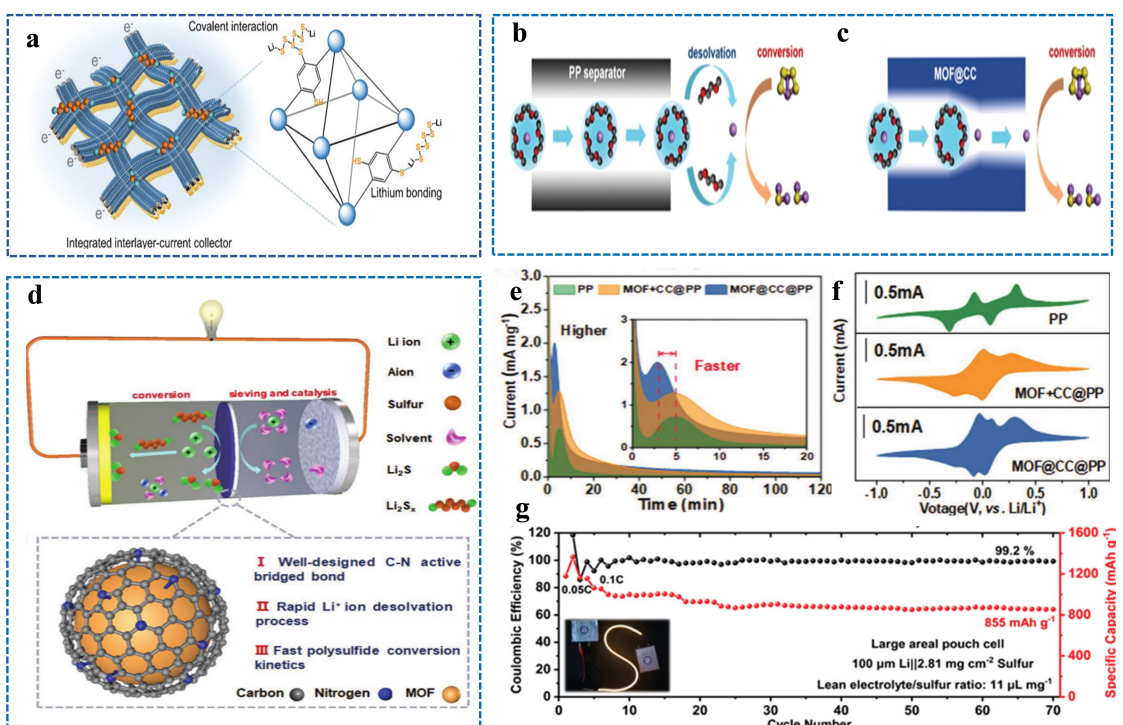


Figure 2. (a) Schematic illustration of the role of CC@UiO-66(SH)₂ in Li-S batteries.^[75] (b) Schematic illustration of the catalytic conversion of MOF@CC@PP diaphragm in a lithium-sulfur battery. Schematic illustration of solvated Li⁺ ions inside (c) a PP separator and (d) MOF channels. (e) Potentiostatic discharge curves of different separators with Li₂S₆ electrolyte at 2.05 V. (f) CV curves of symmetric batteries with Li₂S₆ electrolyte at 0.5 mV s⁻¹. (g) Cycling performance of the large pouch cell using MOF@CC@PP under 2.81 mg cm⁻² at 0.1 C.^[81]

electrolyte ($11 \mu\text{L mg}^{-1}$), with a discharge capacity of 855 mAh g^{-1} after 70 cycles and an average coulomb efficiency (CE) of 99.2%, effectively demonstrating the catalytic desolvation for efficient Li^+ transport kinetics and polysulfide conversion.

Research has shown that nitrogen materials, as catalysts, can promote the reduction and oxidation reactions of sulfur, enhance the reaction kinetics of the electrode, and thus improve the performance of the battery. In view of the basic properties of different doping elements and their different modes of action in the carbon lattice structure, multi-element co-doping is one of the important strategies to regulate the surface chemistry of carbon materials and improve the electrochemical reaction of sulfur.^[84–86] Yin et al. firmly immobilize sulfur components in the form of small sulfur molecules of S_{2-4} within unique 0.5 nm micropores in MOF-derived nitrogen-doped carbon, as a cathode for Li–S battery.^[87] Figure 3a shows the synthesis of MOF-derived C–S hybrids. The obtained samples were treated at 300°C for 1, 2 and 3 hours and were recorded as C–S-1, C–S-2 and C–S-3 respectively. With the increase of 300°C treatment time, the evaporation of sulfur in C–S hybrid surface and mesopore increased. After 3 h of treatment, the micropore volume of all samples was almost zero. Due to the space limitation of 0.5 nm micropores, the size

of S_{5-8} molecules was larger than 0.5 nm and could not exist.^[88] It is reasonable to assume that sulfur exists in micropores in the form of small molecules S_{2-4} . The presence of smaller S_{2-4} molecules in micropores can avoid the formation of higher order polysulfides.^[88,89] As shown in Figure 3b, the C–S-3 hybrid sample has abundant micropores and mesoporous pores. The space limitation of the micropores can effectively trap polysulfide and inhibit shuttle effect. The MOF-derived N-doped carbon mesoporous can effectively alleviate the volume expansion and maintain the stability of the structure. In addition, C–S-3 provides an efficient conductive network, which improves charge transfer dynamics at the electrode-electrolyte interface. Electrochemical tests were conducted to further explore its performance. Compared with C–S-1,2 samples, C–S-3 has relatively higher initial charge-discharge capacity and more stable cycle performance (Figure 3c), and its rate performance is better than the other two comparison samples (Figure 3d). Nitrogen-doped carbon spheres with micropores are obtained by directly carbonizing nitrogen-containing MOF nanocrystals, and sulfur molecules are infiltrated into the microporous carbon spheres to fix smaller sulfur molecules, which has a significant impact on inhibiting the shuttle effect of polysulfide, alleviating volume expansion and improving the electrochemical performance of lithium-sulfur batteries. Qiu and

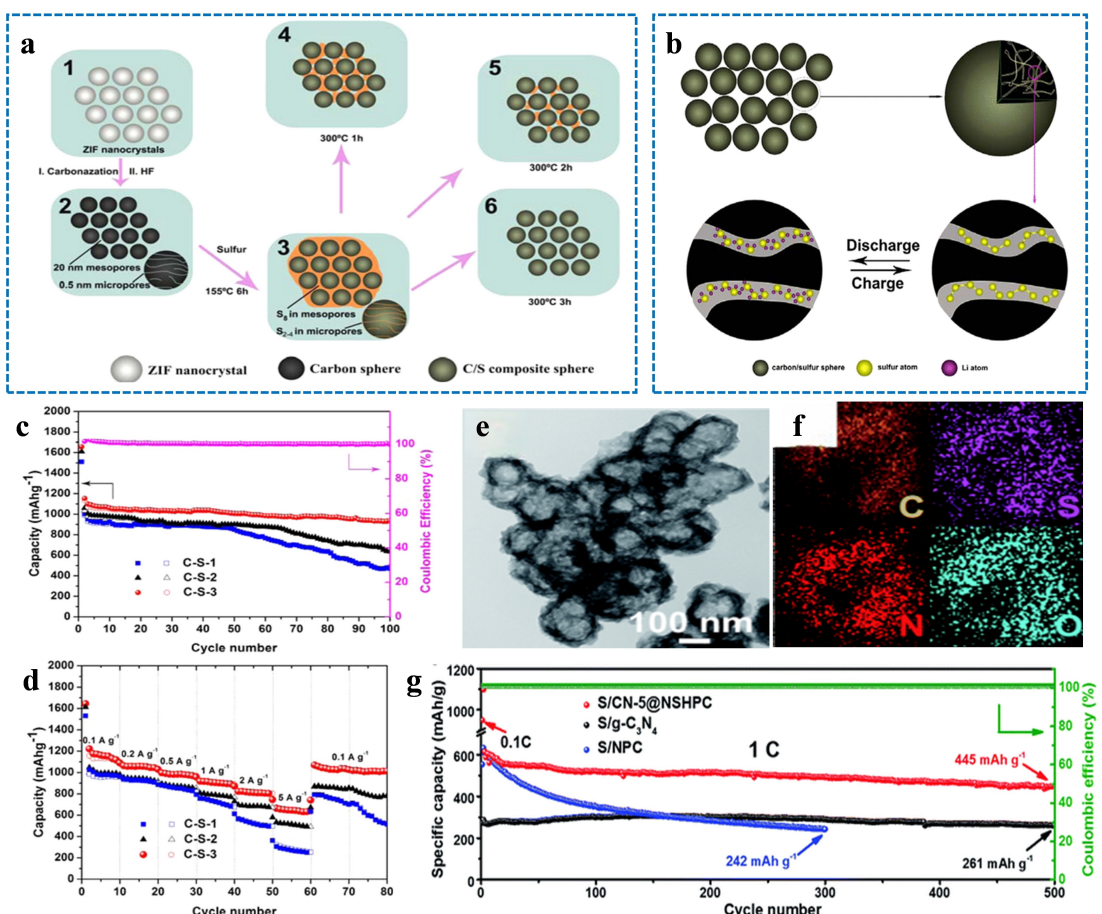


Figure 3. (a) Schematic for Synthesis of C–S Hybrids. (b) Discharge and Charge Mechanism of C–S-3 Hybrid Cathode. (c) Cycling performance of C–S hybrids at 335 mA g^{-1} (pink circles show the Coulombic efficiency of C–S-3 hybrid sample). (d) Rate capability performance of C–S hybrids.^[87] TEM images of (e) CN-5@NSHPC. (f) elemental mapping of CN-5@NSHPC. (g) Cycling performances of S/CN-5@NSHPC, S/NPC and S/g-C₃N₄ tested at a current density of 1 C.^[90]

his colleagues successfully embedded g-C₃N₄ nanodots into N, S co-doped hollow porous carbon shells derived from MOFs(CN@NSHPC) using a dual-solvent strategy.^[90] Figure 3e shows the TEM image of the N and S co-doped hollow porous carbon shell (CN@NSHPC) prepared by a unique double solvent induction strategy. The synergistic effect of the unique hollow design of the carbon shell, N and S co-doping, and nano g-C₃N₄ embedding effectively promotes electron transfer, which can effectively inhibit the shuttle effect of polysulfide. The energy-dispersive spectroscopy (EDS) elemental mapping obtained from the TEM images shown in Figure 3f reveals a good correspondence of the distribution of elements C, N, O, and S, indicating uniform doping of these elements in CN@NSHPC. As can be seen from Figure 3g, the S/CN-5@NSHPC cathode also has a capacity of 445 mAh/g after 500 cycles at 1 C, compared with the S/NPC and S/G-C₃N₄ cathodes. Its cyclic stability and capacity are much higher than those of the other two comparison samples. This proposed strategy provides an insight into a new pathway to construct co-doped carbon hollow nanostructure and nanodot materials by the pore confinement effect. Furthermore, Hu et al. prepared fluorine and nitrogen-doped porous carbon derived from ZIF-8 for use as a membrane modifier to mitigate the shuttle effect and maximize the reutilization of dissolved polysulfides.^[91] Li et al.^[92] reports a multifunctional carbon hybrid with MOFs-derived nitrogen-doped porous carbon anchored on graphene sheets (NPC/G)

serving as a sulfur host. The highly conductive graphene not only provides an interconnected conductive framework to facilitate fast electron transport, but also serves as a building unit to support the MOFs-derived carbon. The rich N and C defects further offer more active sites for strongly adsorbing LiPSs, bridging electron transfer atomic pathway for catalytic reactions to accelerate redox kinetics of Li/S conversion chemistry.^[93] Wang et al.^[94] reasonably designed a layer-by-layer N and P-doped carbon material (MC@CN@CNP), where the sequential doping of N and P altered the electron cloud density on carbon atoms between different layers. The gradient in electron cloud density generated a gradient electric field,^[95,96] which restrained the diffusion of polysulfide anions towards the lithium negative electrode and improved the material's conductivity, enhancing the cycling stability of lithium-sulfur batteries.

Figure 4a is the TEM image of MC@CN@CNP and shows the uniform distribution of C, N, and P elements through element mapping. By controlling the in-situ doping of heteroatoms, a gradient-ordered modified MOF-derived carbon material was obtained, where the different electron cloud densities between layers constitute an internal electric field, beneficial for enhancing the electrochemical reaction kinetics of lithium-sulfur batteries.^[97] Density functional analysis further revealed the impact of layer-by-layer doping of N and P atoms on the electron cloud density of carbon materials. As shown in

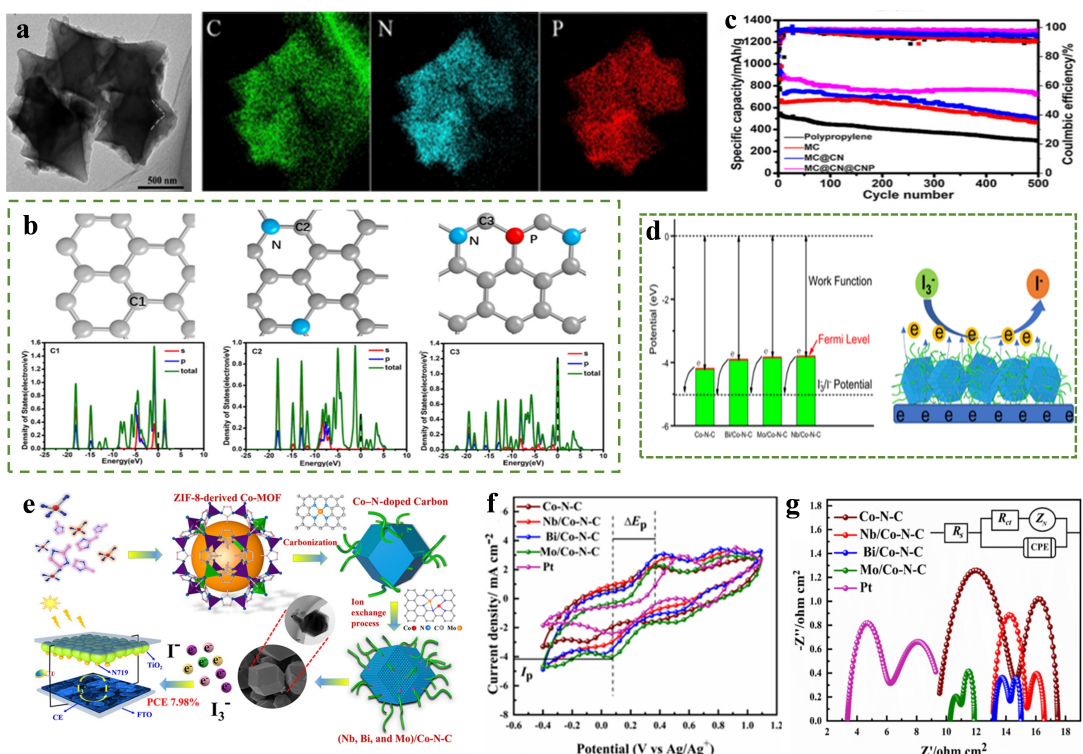


Figure 4. (a) TEM images of MC@CN@CNP and elemental mapping images of C, N and P. (b) The DOS of C1, C2 and C3 in figure, respectively. (c) Cycling performance of Li-S battery based on MC, MC@CN and MC@CN@CNP cathode materials.^[94] (d) Energy level diagram of Co–N–C and (Nb, Bi, and Mo)/Co–N–C compared with the IRR equilibrium potential and electron transformation mechanism among I₃⁻/Nb or Bi or Mo/Co/N–C, where the red line illustrates the possible electron transfer path from CEs to the I₃⁻ in the IRR. (e) Schematic display of the synthesis route of cobalt nitrogen-doped carbon and its coordination with metals (Nb, Bi, and Mo) by ZIF. (f) CV of the as-fabricated CE catalysts at 50 mV s⁻¹. (g) Nyquist plots of symmetrical cells fabricated by using the same CE catalysts and the inset is an equivalent circuit for Nyquist curve fitting.^[102]

Figure 4b, representative C atoms (C1, C2, C3) were selected from the MC, MC@CN and MC@CN@CNP layers respectively. Their DOS values near the Fermi level gradually increased, so the chemical adsorption of S_n^{2-} was enhanced in the electrochemical reaction.^[98] In a word, N and P doping improves the conductivity of MOF-derived carbon, promotes charge transfer, and the porous structure of the material can absorb more electrolyte and enhance the kinetics of ion transport. As a result, Li–S cells exhibit excellent electrochemical properties and cycling stability (Figure 4c). Wu and his colleagues successfully fabricated a novel (Nb, Bi, and Mo)/cobalt-assisted nitrogen-doped carbon nanohybrid derived from ZIF-8^[99–101] with a diamond dodecahedron shape using a simple pyrolysis route followed by ion exchange^[102] (Figure 4d). Heteroatoms such as Co, Cu, and Fe with nonmetal atoms (N and S) doped into carbon along with CNTs provide quick modulation to electrons with superior electronic structures, further enhancing their electrocatalytic behavior.^[103,104] As shown in Figure 4e, the calculated work functions of Co–N–C and (Nb, Bi, and Mo)/Co–N–C are 4.2, 3.8, 3.9, and 3.85 eV, respectively. Their Fermi levels are all higher than the equilibrium potential of IRR (-5.0 eV),^[105] and the work function of (Nb, Bi, and Mo)/Co–N–C is significantly lower than that of Co–N–C and Pt (111) surfaces (5.72 eV),^[106] demonstrating that (Nb, Bi, and Mo)/Co–N–C nanohybrids exhibit higher charge transfer efficiency and catalytic activity compared to Co–N–C nanomaterials. The peak current density (I_p) and peak-to-peak separation (ΔE_p) are key parameters for evaluating the electrocatalytic behavior of all

prepared CE materials based on the CV curves, as plotted in Figure 4f. Comparative analysis shows that the Mo/Co–N–CCE exhibits higher I_p values and lower ΔE_p values, indicating enhanced electrocatalytic behavior and excellent reversibility. The catalytic performance of the prepared CEs was further investigated using electrochemical impedance spectroscopy (EIS) as shown in Figure 4g. The R_{ct} values for Pt, Co–N–C, and (Nb, Bi, and Mo)/Co nitrogen-doped carbon composite are 1.45, 2.54, 1.14, 0.54 and 0.39 Ωcm^2 , respectively. The smaller R_{ct} values indicate faster electron transfer from the electrode surface to the electrolyte, minimizing charge losses at the interface. This demonstrates that the Mo/Co–N–CCE exhibits robust catalytic behavior. This work demonstrates that transition metal/cobalt electrocatalysts with nitrogen-doped carbon networks hold further innovations in the field of electrocatalysis.

Recently, transition metal phosphide (TMP) has attracted widespread interest due to its unique advantages over LSBs.^[107,108] First, TMP shows significant electrical conductivity due to phosphorylated groups with lone pairs.^[109] At the same time, TMP also has excellent catalytic ability, which can not only anchor insoluble LiPSs, but also promote the conversion of polysulfides and accelerate the reaction kinetics.^[110] Fan et al.^[111] successfully prepared Ni/Co phosphides derived from MOFs filled into nitrogen-doped dual-carbon conductive networks (NiCoP@NC), and used them as a modified PP separator for Li–S batteries. Figure 5a shows the SEM image of NiCoP@NC. Due to the unique two-carbon network, NiCoP@NC modified separator

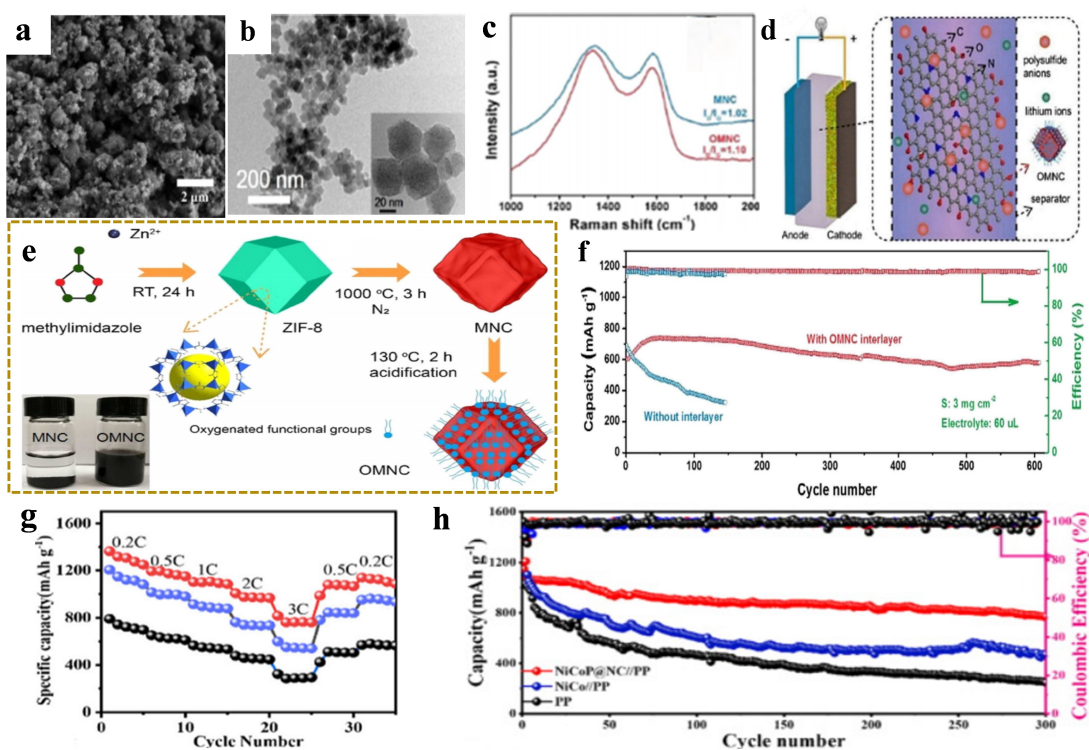


Figure 5. (a) SEM of NiCoP@NC.^[111] (b) TEM images of OMNC.^[112] (c) Raman spectra of MNC and OMNC.^[112] (d) Schematic illustration of the Li–S battery with an OMNC interlayer.^[112] (e) Schematic illustration of the preparation of OMNC nanoparticles. Inset: The dispersity of MNC and OMNC in DOL/DME solution.^[112] (f) Cycling performance at a current rate of 1 C with/without OMNC interlayer with a sulfur loading of 3 mg cm^{-2} .^[112] (g) Rate performance at various rates.^[111] (h) Long-term cyclic performance at 0.5 C.^[111]

can effectively anchor LiPSs, promote the catalytic conversion of LiPSs, and provide a fast channel for lithium ions. First, Ni/Co provides a large number of active sites, hindering the shuttle of LiPSs, and further promoting the redox kinetics of LiPSs as a catalytic site. Secondly, due to the double-carbon conductive network structure and the Co/Ni binary phosphide, the modified diaphragm exhibits abnormal ion/electron conductivity, which accelerates the transmission of Li^+ .^[109] Consequently, the cycle performance, rate performance and capacity of the batteries assembled from NiCoP@NC modified separator were greatly improved (Figure 5h). In addition, Li et al. proposed an oxygen-containing metal-organic framework (MOF)-derived nitrogen-doped microporous carbon (OMNC) interlayer to mitigate the shuttle effect of polysulfides.^[112] The TEM image (Figure 5b) clearly shows the presence of several graphene layers stacked parallel to the edges of the nanoparticles. These microporous structures and graphene layers can provide a three-dimensional electron transport pathway while promoting ion transport. Figure 5e shows the schematic diagram of the preparation process of OMNC. A large number of carboxyl and hydroxyl functional groups are grafting on the prepared OMNC sample, which enables OMNC, as separator, to not only effectively adsorb polysulfides through synergistic physicochemical effects, but also to promote electron transfer as a second fluid collector and increase the utilization rate of active substances. The Raman spectra of OMNC and MNC nanoparticles both exhibit two peaks: the D band at 1340 cm^{-1} and the G band at 1582 cm^{-1} (Figure 5c). The G band is characteristic of graphitic carbon, while the D band corresponds to disorder and defects in the carbon structure.^[113] As shown in Figure 5d, the OMNC separator is applied in the structure of the Li–S battery. Due to the adsorption between OMNC layers, the polysulfide anions are confined to the cathode side, effectively suppressing the shuttle effect of polysulfides. Figure 5f compares the cycling performance with and without the OMNC separator, showing that the battery with the OMNC interlayer exhibits excellent cycling stability and high Coulombic efficiency. Hence, the simple synthetic strategy of the functional OMNC interlayer shows great promise as an approach to the capture and reutilization of polysulfides.

The research results of the above team show that the non-metallic support can improve the conductivity of the active substance S, enhance the physicochemical confinement ability of polysulfides and ion transport kinetics, and have a significant effect in inhibiting the shuttle effect, that is, it can effectively improve the cycling stability of lithium-sulfur batteries.

4.2. Doping of Single Metal into MOF

At present, the active site of MOF is relatively single, and in the context of electrochemistry, various metals and metal-containing compounds are often used to increase the rate of electrochemical reactions due to their high catalytic activity.

Arava and colleagues investigated the electrocatalytic effect of the noble metal catalyst Pt on the redox reaction of LiPSs.^[114] In addition to precious metals, transition metals also have high

catalytic activity in many electrochemical reactions. Dong et al.^[115] synthesized a novel cobalt-based metal-organic framework sulfur host and nitrogen-doped graphite carbon (Co–N–GC), successfully achieving catalysis of sulfur redox reactions, capture of polysulfides, and an ideal electron matrix (Figure 6c). Figure 6a further confirms the distribution of element S in the composite material. The elemental distribution map on the S@Co–N–GC particles not only clearly reveals the uniform distribution of S on the surface of Co–N–GC, but also confirms the uniform presence of Co nanoparticles and the effective incorporation of N atoms into the carbon matrix. Due to the presence of Co, it is proved that Co (II) has a strong interaction with polysulfides, and the synergistic effect of Co–N can also show that Co–N–GC composites have a dual catalytic effect on the redox of S. The S@Co–N–GC composite electrode shows excellent cycling stability, with no significant voltage degradation even after 500 cycles (Figure 6g). Wang et al. reduced graphene oxide (RGO) wrapped metal-organic frameworks (MOFs) derived cobalt doped porous carbon polyhedrons synthesized via a carbonization process, are for the first time used for sulfur immobilizers (RGO/C–Co–S) as cathodes for high performance Li–S batteries.^[116] The research results indicate that the high conductive carbon matrix with Co particles ensures fast charge transfer processes, resulting in good rate capability. Jiao and colleagues developed a porous nano-polyhedron metal-organic framework structure (CrP@MOF).^[117] The unique porous structure of the polar CrP@MOF polyhedral surface helps to crosslink LiPSs (Figure 6b), thereby improving the utilization of sulfur. The analysis in Figure 6d shows that the precursor based on Cr-based MOF has a high specific surface area and abundant catalytic adsorption sites, which can enhance the adsorption of polysulfides, suppress the shuttling of polysulfides, and thereby accelerate the redox kinetics between polysulfides. The PDOS shown in Figure 6f indicates that the Cr 3 d band crosses the Fermi level, suggesting that CrP has good conductivity and facilitates charge transfer for LiPS conversion. Additionally, as shown in Figure 6e, during the discharge-limiting step from Li_2S_4 to Li_2S_2 , the change in free energy for CrP (0.91 eV) is lower than that for Cr_2O_3 (1.13 eV), implying that the reduction of sulfur on CrP is thermodynamically more favorable compared to Cr_2O_3 .^[118,119] The long-term cycling performance graph shown in Figure 6h at 1 C rate demonstrates the improved cycling stability of CrP@MOF material due to its high catalytic activity. This work provides an advanced strategy for suppressing shuttle effects and accelerating LiPS catalytic conversion. Liu et al. developed titanium-containing metal-organic skeleton modified membranes for use in new lithium-sulfur batteries.^[120] Figure 7a shows the schematic diagram of MIL-125 (Ti) modified PP/PE diaphragm in lithium-sulfur battery. This titanium metal-organic skeleton (MOF) containing MIL-125 (Ti) has an open skeleton structure, high inherent microporosity and lewis acid properties. The particle size falls within the range of $1.5\text{--}2\text{ }\mu\text{m}$ in diameter, with a large surface area ($1386\text{ m}^2\text{ g}^{-1}$), and a three-dimensional open framework of MOF particles consisting of uniform micropores, ensuring rapid transport of Li^+ ions and facilitating uniform Li plating/stripping.^[121,122] Also, the strong binding ability between O atoms from the BDC

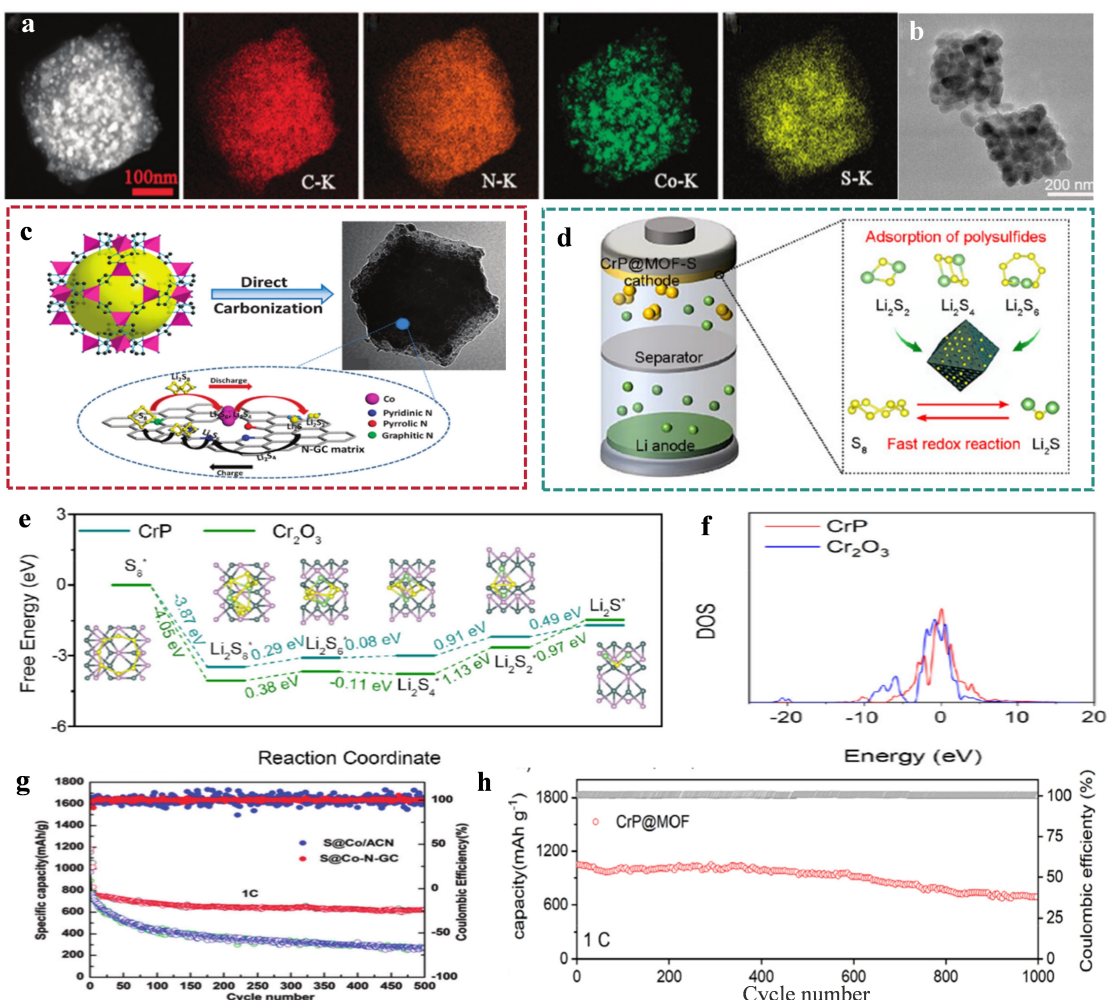


Figure 6. (a) The HAADF-STEM image of the S@Co-N-GC composite and the corresponding elemental mapping of C, N, Co and S.^[115] (b) TEM image of CrP@MOF.^[116] (c) Schematic illustration of a dual-catalyst anchored Co-N-GC composite preparation and its interaction with polysulfides during the charge/discharge processes of a Li-S battery.^[115] (d) Schematic diagram of the catalytic conversion of polysulfides by the porous MOF structure-based CrP nanocatalyst.^[116] (e) Gibbs free energy profiles of various PS on CrP. (f) PDOS for Cr 3 d states of CrP and Cr₂O₃.^[116] (g) Cycling performance and coulombic efficiency comparisons between the S@Co-N-GC and the S@Co/ACN composite electrodes at 1 C.^[115] (h) Long-term cycling test of the CrP@MOF cathode.^[116]

ligands in MIL-125 (Ti) and Li⁺ ions in Li_nS_n leads to the immobilization of S_n²⁻.^[123-125] Figure 7c-d investigate the adsorption experiment of MIL-125 (Ti) on polysulfides. The strong binding affinity between the O atoms from the BDC ligand in MIL-125 (Ti) and the Li⁺ ions in Li₂S₆ effectively suppresses the shuttle effect in lithium-sulfur batteries. Therefore, the Li-S battery with MIL-125 (Ti)-PP/PE membrane exhibits higher sulfur utilization efficiency, thus demonstrating high cycling stability (Figure 7f). In recent years, Qiu et al. have proposed a general metal-organic framework (MOF) confinement strategy to prepare atomically dispersed metal catalysts ADMCs (named MOF-808-M, M= Fe, Co, Ni, Cu, Zn, etc.) with the help of ethylenediaminetetraacetic acid (EDTA).^[126] Figure 7b shows the optimized structures of LiPS and Li₂S adsorbed on various MOF-based electrocatalysts. The benefits of the M-N₂O₂ sites in MOF-808-M for achieving LiPS capture and rapid redox kinetics are further explored. In addition, the sulfur reduction reaction (SRR) and antili₂s dissociation processes were simulated to gain a deeper understanding of the catalytic activity of the M-N₂O₂ site

in MOF-808-M. As shown in Figure 7e, MOF-808-M significantly increased the free energy during the liquid-solid transformation of LiPSs, indicating that electrocatalysis at the active site would effectively promote the Redox kinetics of polysulfides. The long-cycle performance test of these MOF-808-M cathodes at 1 C clearly shows that the introduction of M-N₂O₂ site in MOF-808-M can not only increase the specific capacity by about 51%, but also enhance the long-cycle stability of lithium-sulfur batteries (Figure 7g). This work provides a reference for the precise design of ADMCs with well-defined coordination structures to enhance the adsorption behavior of LiPSs and their catalytic activity.

In addition to transition metals, we also explored the research progress of other metal-doped MOFs on the catalytic conversion of polysulfides in lithium-sulfur batteries. Hong et al. used cerium-based MOFs combined with carbon nanotube as the separator coating material to catalyze the conversion of polysulfides.^[127] Xiong et al. prepared a layered functional layer composed of a lithium-ion-inserted ZIF-67 (Li-MOF) layer and

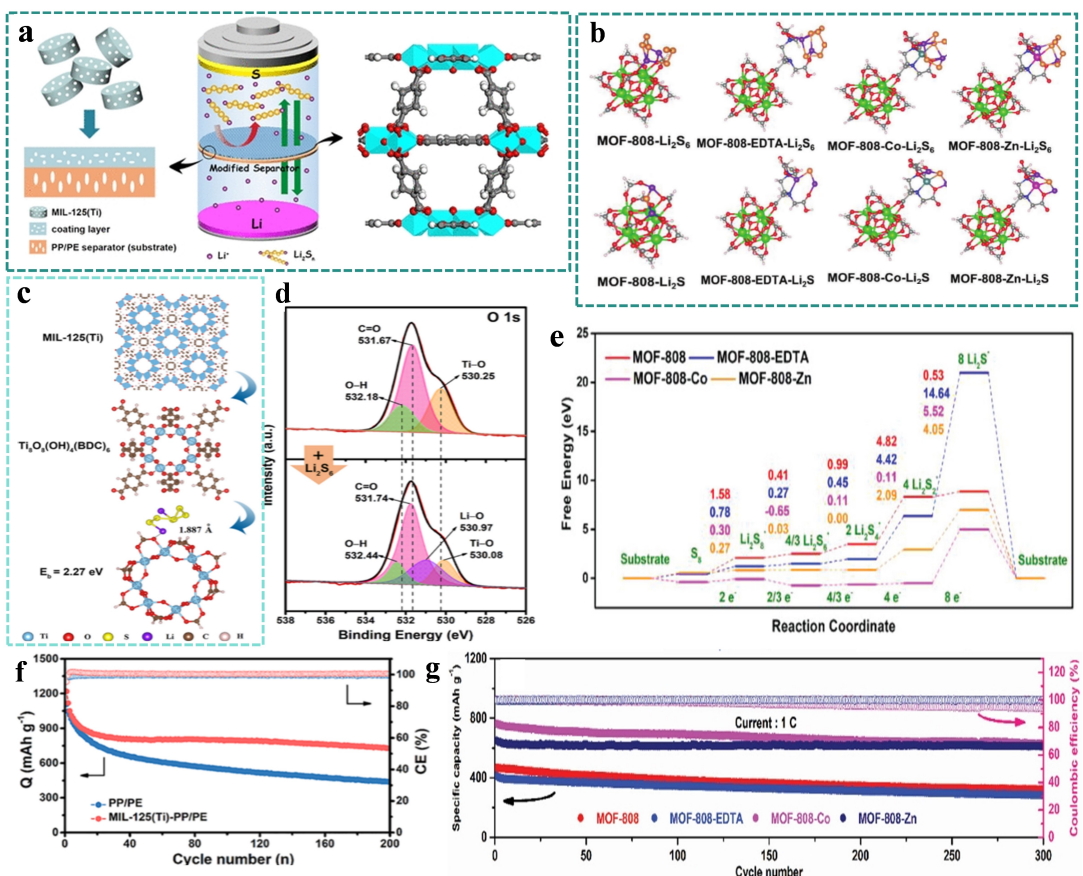


Figure 7. (a) Schematic illustration of the Li-S battery with the MIL-125 (Ti)-modified PP/PE separator.^[120] (b) The optimized configurations of Li₂S₆ and Li₂S species adsorbed on MOF-808, MOF-808-EDTA, MOF-808-Co, and MOF-808-Zn based on DFT calculations.^[126] (c) Optimized stable structure of adsorption configuration between Li₂S₆ and MIL-125 (Ti).^[120] (d) High-resolution O 1 s XPS spectrum of MIL-125 (Ti) before and after adsorption of Li₂S₆.^[120] (e) free energy profiles for the SRR on MOF-808, MOF-808-EDTA, MOF-808-Co, and MOF-808-Zn substrates at the equilibrium potential.^[126] (f) cyclic performance at 0.2 C.^[120] (g) long-term cycling performance at 1 C.^[126]

reduced graphene oxide (RGO) layer (Li-MOF/RGO). The Li-MOF layer ensures rapid ion transfer across the modified separator membrane, providing efficient trapping of polysulfides and enhanced conversion kinetics, thereby preventing polarization due to ion depletion. Over 600 cycles at 1 C, the decay rate was only 0.089% per cycle, offering a more promising strategy for achieving high-performance lithium-sulfur batteries.^[128] Guan et al. successfully synthesized Ce-Uio-66-NH₂ (Ce-MOF) complexes and designed multifunctional diaphragm coatings for high-performance Li-S batteries.^[129] Figure 8a presents the SEM image of Ce-MOF and the corresponding elemental mapping images, revealing that the elements C, N, O, and Ce are uniformly distributed on the surface of Ce-MOF. The Ce⁴⁺ metal sites in the Ce-Uio-66-NH₂ (Ce-MOF) exhibit Lewis acidic characteristics and the sulfur with lone-pair electrons exhibit soft Lewis basic property; therefore, the Ce-MOF could interact with a polysulfide strongly and facilitating the redox reaction of polysulfides.^[130] The Ce-MOF/Super-P based separator effectively prevents the migration of polysulfides to the lithium anode while allowing the passage of Li⁺ ions, thereby inhibiting the shuttle effect (Figure 8c). In addition, the amine groups in the Ce-MOF could also interact associatively with the polysulfides,^[131,132] which act synergistically with the metal sites

to inhibit the polysulfides migration. Therefore, compared with other separators, Ce-MOF materials have higher utilization of active substances and excellent magnification properties (Figure 8f). Furthermore, Zhang and his colleagues prepared a continuously crystallized zirconia-based MOF-808 film on carbon nanotube films using surface in-situ hydrothermal method as a multifunctional interlayer material for lithium-sulfur batteries^[133]. From the cross-section view (Figure 8b), the dense and tightly bonded MOFs layer is tightly covered on the CNT support with a thickness of 1.9 microns, and the total thickness of the composite film is about 8–9 microns based on the thickness of the CNT film. As an intermediate layer, MOF-808 membrane can act as an ion screen to selectively block LiPSSs and ensure the rapid passage of Li ions (Figure 8d). In addition, the redox kinetics is also accelerated by MOF-808/CNT. The long-term cycling performance of different interlayers is shown in Figure 8e. The retention rate of MOF-808/CNT interlayers after 500 cycles (755.5 mAh g⁻¹) at 1 C is 83.2%, and the cycle decay rate is only 0.03%. The superior rate performance of MOF-808/CNT can be attributed to enhanced ion transfer and accelerated sulfur redox reactions.^[134,135] This study provides an innovative idea for the preparation and application of MOFs films, especially in energy storage devices.

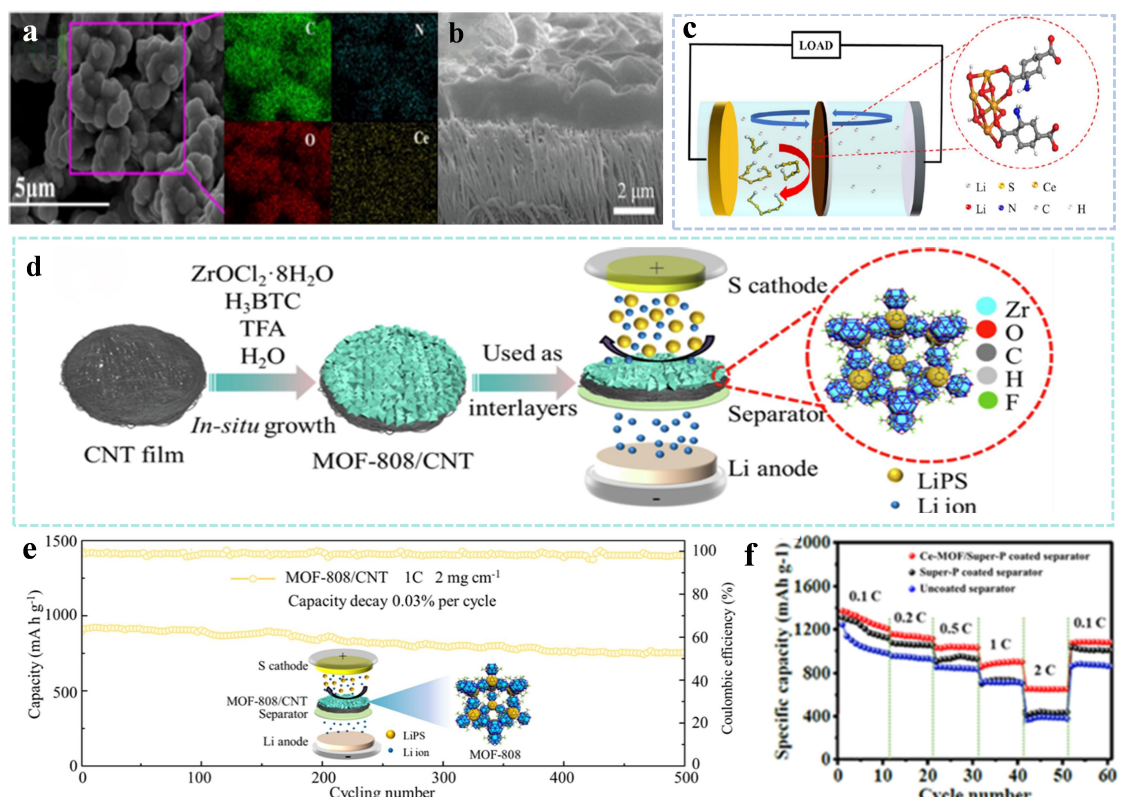


Figure 8. (a) SEM and elemental mapping of the Ce-MOF.^[129] (b) Cross-section SEM of MOF-808 membrane.^[133] (c) Schematic illustration of Ce-MOF/Super-P coated separator for blocking lithium polysulfides migration to the lithium anode in the Li–S batteries.^[129] (d) Schematic illustration of MOF-808/CNT interlayer.^[133] (e) Long cycle performance diagram of MOF-808/CNT separator at 1 C with S loading of 2 mg cm⁻².^[133] (f) The rate performance from 0.1 C to 2 C of the Li–S batteries with three different separators.^[129]

These results show that metal catalysts can greatly enhance the electrochemical redox reaction kinetics in lithium-sulfur batteries. More importantly, these metals have high electronic conductivity, which can significantly improve the sulfur utilization rate, inhibit the polysulfide shuttle effect, and improve the electrochemical performance of Li–S batteries.^[136] While single-atom catalysts have a high utilization rate, they have a relatively low mass density in the body.^[137] Therefore, it is imperative to develop sulfur-based materials to realize the multi-step and two-way catalysis of sulfur species, and to improve the electrochemical performance of lithium-sulfur batteries.

4.3. Bimetal-Doped MOF

To accelerate the electrochemical kinetics of sulfur reactions, researchers have studied various catalytic materials, such as different MOFs, transition metal elements, and their compounds, which can catalyze the conversion of sulfur species after anchoring LiPSs. However, the activity of a single adsorbent or catalyst is limited to a certain extent, and it is difficult to achieve simultaneous adsorption and conversion of multiple LiPSs in complex environments. Excessive adsorption intensity will significantly increase the energy barrier of conversion between soluble LiPSs, which is not conducive to the desorption and rapid transformation of LiPSs. Therefore, it is

very important to establish a synergistic mechanism of “strong adsorption” and “fast conversion” of LiPSs for the application of high-performance Li–S batteries.^[138]

The regulation of sulfur precipitation by cathode materials includes inhibition of the shuttle effect of LiPSs and enhancement of redox reaction kinetics, which are represented by adsorption capacity and electrocatalytic activity, respectively.^[139] The adsorption capacity indicates the ability of a material to capture LiPSs and is characterized by polarity. Due to the difference in electronegativity between Li and S atoms, LiPSs species are classified as polar molecules.^[140] In general, bipolar intermolecular interactions are stronger than intermolecular interactions with non-polar ones, which explains why non-polar carbons exhibit limited absorption capacity for polar LiPSs (Figure 9a). Metal-based materials, on the other hand, are inherently polar and, therefore, show stronger interactions with LiPSs than non-polar carbons. Once the LiPSs are anchored to the surface of the metal-based material, chemical bonds may be formed, and this strong chemical interaction prevents the LiPSs from diffusing into the electrolyte, thus inhibiting the shuttle effect (Figure 9b). In addition, the high conductivity of the electrocatalyst is beneficial for accelerating the charge transfer kinetics, thereby increasing the reaction speed. Therefore, sulfur hosts with high electrocatalytic activity can catalyze the deposition and decomposition of Li₂S, promote sulfur precipitation, and reactivate solid discharge products,^[141] as

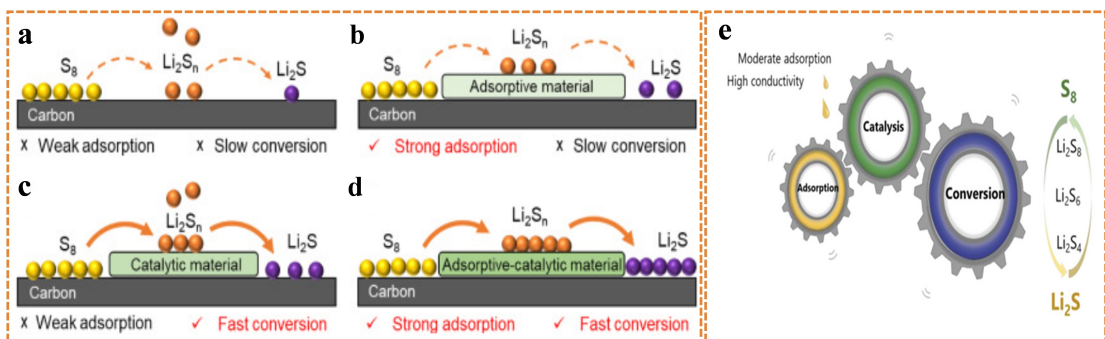


Figure 9. Adsorption-catalysis synergistic effect. (a) Carbonaceous materials showing weak adsorption capability and poor catalytic activity. (b) Adsorptive materials showing strong adsorption capability but poor catalytic activity. (c) Catalytic materials showing high catalytic activity but weak adsorption capability. (d) Adsorptive and catalytic materials showing adsorption-catalysis effect toward sulfur evolution reactions.^[141] (e) The function and basic mechanism of adsorption, catalysis, and conversion.^[142]

shown in Figure 9c. Eventually, the adsorption and catalysis of the sulfur body will form a coordination mechanism to improve the reaction kinetics of sulfur to effectively regulate the precipitation of sulfur (Figure 9d). From Figure 9e, the adsorption characteristics and catalytic conversion behaviors of lithium polysulfides (LiPSs) in lithium-sulfur chemistry are observed to interact rather than exist independently.^[142]

Bimetallic materials usually have unique advantages, which can form a fast "adsorption-catalysis" interface for the conversion of LiPSs, effectively prevent the accumulation of LiPSs on the cathode surface during the charging process, thereby significantly improving its utilization rate, and realize the synergistic mechanism of adsorption catalysis by forming a more stable interface transition.

Zhou et al.^[143] combined ZnPd and Pd-ZIF-8 with CNT through carburizing treatment to prepare ZnPd/NCF. The TEM image in Figure 10a shows ZnPd alloy particles doped in porous carbon. In the elemental distribution map (Figure 10b), it can be observed that C, Zn, Pd, and N elements are uniformly distributed in ZnPd/NCF, confirming the successful doping of ZnPd alloy particles in the derived material. Figure 10e explores the catalytic activity of the ZnPd alloy composed of the lithium philophile element Zn and the sulfur philophile element Pd towards lithium polysulfides. From the figure, we can analyze that ZnPd/NCF can enhance the redox kinetics of lithium polysulfides, accelerating their catalytic conversion. As a result, ZnPd/NCF could rapidly adsorb and catalyze lithium polysulfides at high sulfur loadings or current densities, enabling lithium-sulfur batteries with excellent rate performance (Figure 10i). This work provides useful information for exploring the design of high-efficiency catalysts for lithium polysulfides. Xu et al.^[144] prepared a novel Al/Cu-MOF cathode material by uniformly dispersing Cu²⁺ in Al-MOF using a one-step hydrothermal method, its topography is shown in Figure 10c-d, showing a quasi-rectangular shape. Zhou and co-workers utilized Cu₃(BTC)₂@GO as an interlayer to construct ionic sieve membranes.^[145] Therefore, in recent years, Cu²⁺ has been considered an effective metal ion for anchoring polysulfides due to its affinity for sulfur. Compared with traditional porous carbon host materials, the metal nodes (Lewis acidic sites) and

the porous structure, resulting from the connecting organic functional groups, can provide effective binding sites for the lithium polysulfides and strongly confine them within the MOF pores.^[146–148] The interaction mechanism in the main material of Al-MOF and Al/Cu-MOF is shown in Figure 10f. Compared with Al-MOF, Li₂S_x and S_n²⁺ have stronger binding energy and lower steric hindrance, and Cu²⁺ is more likely to capture Li₂S_x molecules. Further, DFT calculations were employed to gain a deeper understanding of the improved performance of Al/Cu-MOF in lithium polysulfide adsorption. By observing the complex structure of MOF-Li₂S₈ in Figure 10g-h, it was deduced that the enhanced interaction can be attributed to the replacement of the lower-valent Cu²⁺ by higher valent Al³⁺ induces an internal dipole which contributes to the framework-polysulfides interaction. The results indicate that the cycling performance and rate capability of the Li-S batteries assembled with Al/Cu-MOF-S have been significantly improved (Figure 10j). This provides a new and effective pathway for the preparation of efficient sulfur-based materials. Based on the excellent properties of cationic MOFs, Zhang et al. proposed the preparation of Cu–Mo nanoparticles embedded in multifunctional independent nitrogen-doped porous carbon nanofibers (Cu–Mo@NPCN) by the exchange of cationic MOFs with MoO₄²⁻ anions.^[149] Recent research indicates that copper (Cu) can form a chemical bond with sulfur, preventing the dissolution of LiPS during cycling.^[150] Molybdenum (Mo), as one of the most popular transition metals, can serve as an efficient catalyst toward LiPS because of its controllable structure and variable Mo central valence.^[151–153] Figure 11a shows the preparation of Cu–Mo bimetallic nanoparticles in free-standing nitrogen-doped porous carbon nanofibers with high catalytic sites and high sulfur content based on transition metal framework anion exchange (Cu–Mo@NPCN). Compared with the single metal Cu@NPCN, the bimetallic Cu–Mo@NPCN composite has more active sites, so it has stronger adsorption capacity and better catalytic activity. The interconnected porous channels in Cu–Mo@NPCN allow for rapid electron/Li⁺ transfer, endowing the composite with excellent conductivity (Figure 11b). The oxidation of solid Li₂S was also studied through constant potential charging process. The results confirmed that the Cu–Mo@NPCN catalyst

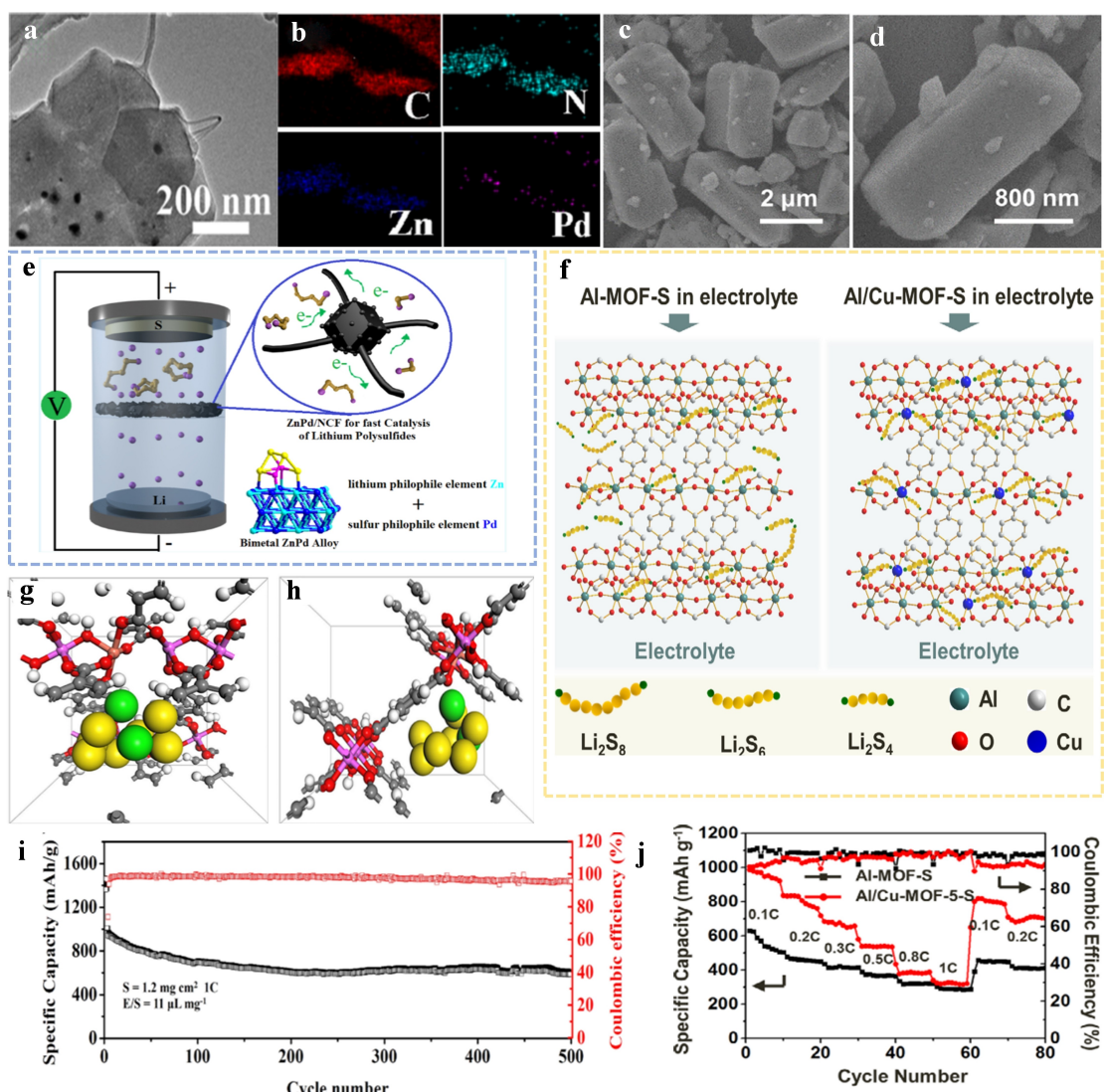


Figure 10. (a) TEM image of ZnPd/NCF.^[143] (b) Energy dispersive X-ray spectroscopy (EDX) elemental mapping of carbon, nitrogen, zinc, and palladium in ZnPd/NCF.^[143] (c-d) SEM images of Al/Cu-MOF-5-S.^[144] (e) Schematic diagram of rapid adsorption and catalysis of ZnPd/NCF separator in lithium-sulfur batteries.^[143] (f) Schematic illustration for the lithium polysulfides binding with Al-MOF and Al/Cu-MOF.^[144] (g-h) Different views of the structure of the Al/Cu-MOF-Li₂S₈ complex.^[144] (i) Long cycle life of ZnPd/NCF at 1 C and 1.2 mg cm⁻² sulfur mass loading.^[143] (j) Rate performances of Al-MOF-S and Al/Cu-MOF-5-S with the corresponding coulombic efficiencies at different discharge rates.^[144]

synergistically reduced the overpotential of LiPS conversion, promoting the redox kinetics of sulfur species. Thus, the freestanding Cu–Mo@NPCN/S cathodes have achieved high volumetric/areal capacities and long cycling life even under high sulfur loadings and current rates (Figure 11e). Lu's team^[154] proposed an effective strategy for core-shell Co/Ni bimetal-doped metal-organic framework (MOF)/sulfur nanoparticles to address slow dynamic mechanics and shuttle effects (Figure 11c). Integrating MOF ("net") and sulfur nanoparticles (SNP) ("fishes") into a core-shell structure, where the MOF shell overgrows on the surface of sulfur species, and prevents the MOF from forming single particles due to self-nucleation tendencies.^[155] According to wavelet transform (WT) calculations of the corresponding K-edge EXAFS spectra (Figure 11d), it is indicated that the sulfur nanoparticles (SNP) in S@MOF nanocomposites are confined within the MOF through Co–O/S and

Ni–O/S bonds and spatial constraints. This not only alleviates the shuttling of LiPS but also ensures faster cation transfer within the designed nano-platform. Long-term cycling tests were conducted at a high sulfur loading of 0.2 C, further demonstrating the superior electrocatalytic capability of the dopants for the entire sulfur redox reaction (SRR), effectively accelerating the reaction kinetics and enhancing sulfur utilization (Figure 11f). In addition, Deng et al.^[156] developed a novel, cost-effective 3D Fe-ZIF-8 modified diaphragm with design capabilities to achieve the synergistic effect of blocking and catalytic conversion of soluble polysulfides to prevent the shuttle effect of Li–S batteries. The morphology of Fe-ZIF-8 was observed to be a nano-flower structure through electron microscopy images (Figure 12a). Figure 12d explores the inhibitory effect of the modified separator on the shuttling of soluble polysulfides. Figure 12g evaluates the long-term cycling per-

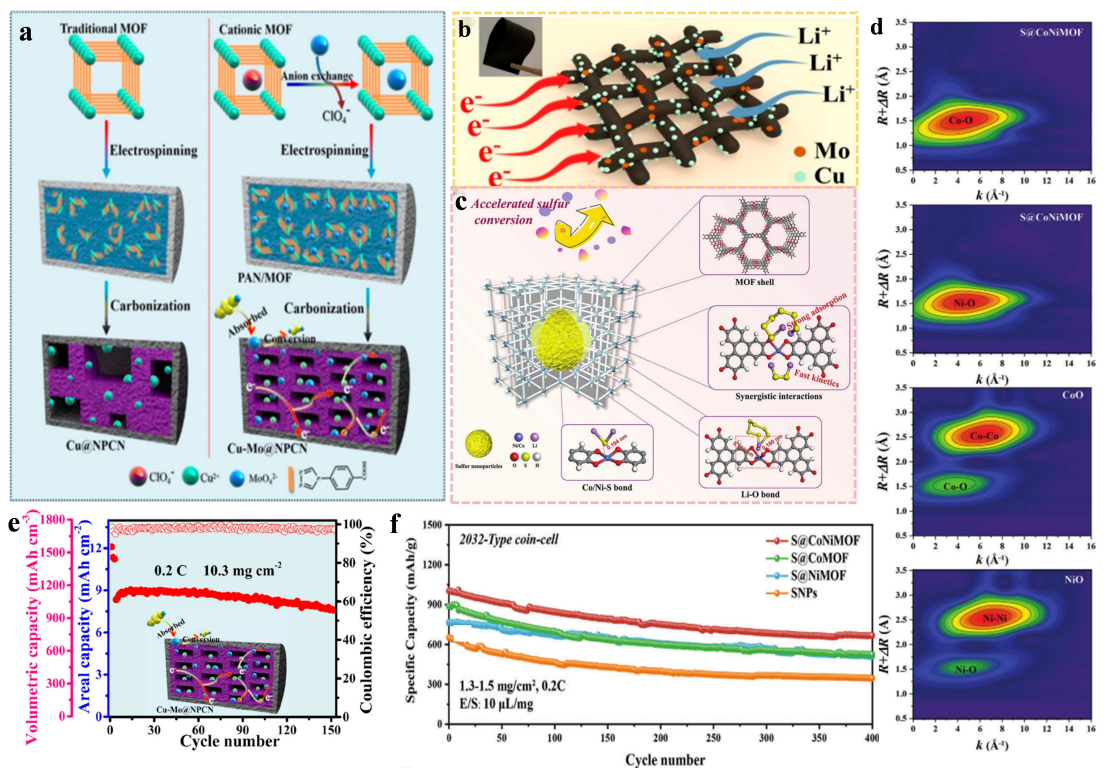


Figure 11. (a) Schematic illustration for the preparation of the Cu–Mo@NPCN/S and its corresponding charge/discharge process.^[149] (b) Illustration of ion/electron transfer in Cu – Mo@NPCN composite.^[149] (c) Schematic illustrating the “fish-in-net” encapsulation of sulfur nanoparticles and the amplification of multiple interactions including physical confinement, covalent bonding, and coordination bonding in the obtained nanocomposite.^[154] (d) Wavelet transform (WT) analysis performed using the EXAFS spectra for different samples.^[154] (e) Cyclic performance curve of Cu–Mo@NPCN cathode at a high sulfur load of 0.2 C.^[149] (f) long-time cycling performance at 0.2 C.^[154]

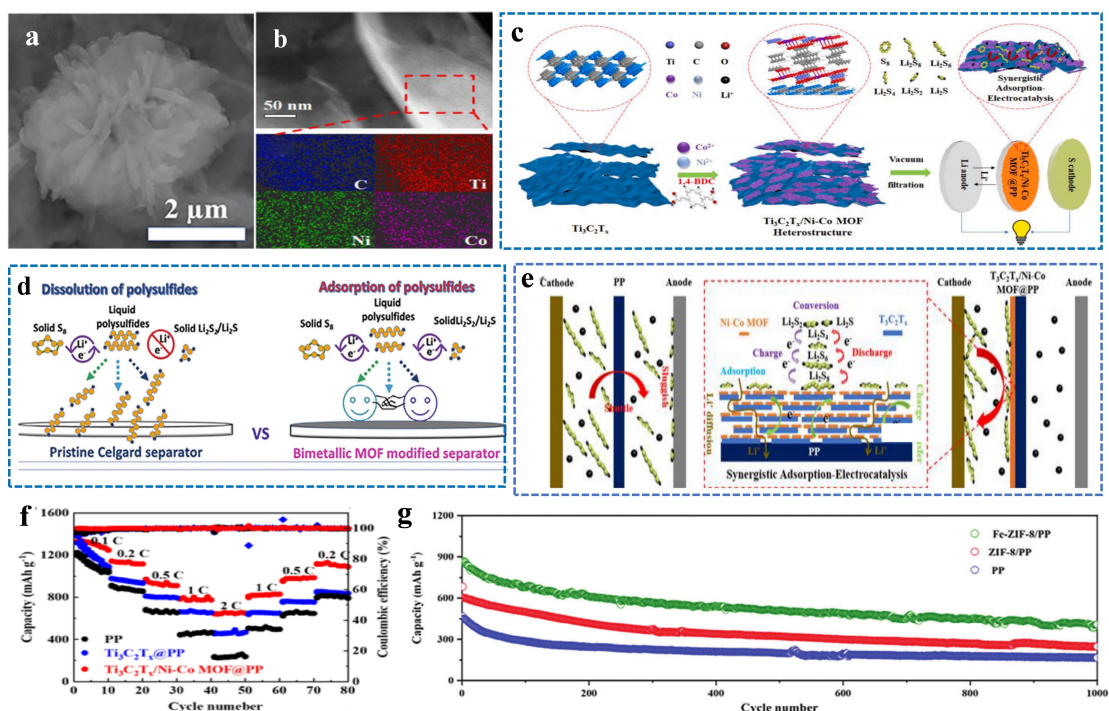


Figure 12. (a) SEM images of Fe-ZIF-8.^[156] (b) HAADF-STEM image and the corresponding elemental mappings recorded from the Ti₃C₂T_x/Ni–Co MOF product.^[163] (c) Schematic illustration for the synthesis of 2D/2D Ti₃C₂T_x/Ni–Co MOF heterostructure.^[163] (d) Schematics of the polysulfides permeation by PP and MOF modified separators.^[156] (e) Schematic illustration of discharging/charging process of Ti₃C₂T_x/Ni–Co MOF@PP.^[163] (f) rate performance of Li–S batteries with PP, Ti₃C₂T_x@PP and Ti₃C₂T_x/Ni–Co MOF@PP separator.^[163] (g) Long-term cycling performance of the Li–S batteries at 0.5 C.^[156]

formance of different separators, and Fe-ZIF-8/PP exhibits a high cycle life with 1000 cycles and reaches 409 mAh g^{-1} after 1000 cycles. Furthermore, Dong et al. used Mn doping to prepare bimetallic MOFs MIL-101 (Cr) as a sulfur-containing cathode.^[157] MIL-101 (Cr) possesses certain catalytic properties due to the presence of Cr.^[158,159] Both Mn and Cr have exhibited excellent catalytic performance in different cells^[160,161] and synergistic interactions between Cr and Mn oxides due to electron migration can lead to enhanced catalytic activity.^[162] This research provides a novel approach for preparing efficient sulfur-containing materials for LSBs. Tang et al. developed a novel 2D/2D heterostructure consisting of ultrathin Ni1–Co MOFs containing unsaturated metal sites and conductive $\text{Ti}_3\text{C}_2\text{T}_x$ nanosheets ($\text{Ti}_3\text{C}_2\text{T}_x/\text{Ni–Co MOF}$).^[163] Figure 12c shows the preparation process diagram of 2D/2D $\text{Ti}_3\text{C}_2\text{T}_x/\text{Ni–Co MOF}$ heterostructure. Among them, the $\text{Ti}_3\text{C}_2\text{T}_x$ nanosheet acts as a conductive substrate to provide electrons for Ni–Co MOFs and activate unsaturated metal sites to catalyze and transform LiPSs. At the same time, the ultra-thin Ni–Co MOF prevents the $\text{Ti}_3\text{C}_2\text{T}_x$ nanosheets from being restacked. Therefore, the heterogeneous structure has a synergistic effect of adsorption-electrocatalysis on polysulfide lithium on the membrane of lithium-sulfur battery. Figure 12b shows the TEM image of the heterostructure, and corresponding elemental mapping also indicates the uniform distribution of C, Ti, Ni, and Co in the $\text{Ti}_3\text{C}_2\text{T}_x/\text{Ni–Co MOF}$. Exploring the discharge/charge process of $\text{Ti}_3\text{C}_2\text{T}_x/\text{Ni–Co MOF@PP}$ (Figure 12e), it can be seen that ultra-thin Ni–Co MOFs with abundant unsaturated metal sites can anchor LiPSs and promote their transformation, while the high electrical conductivity of $\text{Ti}_3\text{C}_2\text{T}_x$ nanosheets provides a large number of electrons to accelerate the reaction kinetics. The ability of heterostructure to fix and catalyze the transformation of LiPSs was demonstrated. The $\text{Ti}_3\text{C}_2\text{T}_x/\text{Ni–Co MOF}$ heterostructure functional separator endows lithium-sulfur batteries with superior electrochemical performance, manifested by excellent cycling stability and rate capability (Figure 12f). This work provides a direction toward developing advanced 2D/2D heterostructures modified separators for high-performance Li–S batteries.

The above experimental results show that the introduction of a second active metal site as an electrocatalyst for the electrocatalytic conversion of enclosed or adsorbed polysulfides into active materials is an effective solution. It was demonstrated that the doping of bimetals in MOFs can achieve the synergistic effect of blocking and catalytic conversion of soluble polysulfides to prevent shuttle in rechargeable Li–S batteries, while allowing free and uniform transport of lithium ions, ultimately optimizing the electrochemical performance of Li–S batteries.^[156]

Based on the above analysis, the effectiveness of MOF doping strategies in mitigating the shuttle effect largely depends on the type of doping and the specific MOF structure. Non-metallic dopants generally provide beneficial effects but may not be sufficient alone to completely suppress the shuttle effect. Single-metallic dopants offer significant improvements but may face issues related to metal leaching and long-term stability. Dual-metallic doping appears to offer the most

promising approach by combining the advantages of different metals, though it introduces complexity in synthesis and optimization. In summary, while MOF doping (whether non-metallic, single-metallic, or dual-metallic) has shown potential in improving the catalytic conversion of polysulfides, a comprehensive understanding of the underlying mechanisms and long-term performance remains crucial. Future research should focus on optimizing the doping strategies, enhancing the stability of MOFs, and exploring novel materials to achieve better suppression of the shuttle effect in Li–S batteries. Table 3 summarizes the advantages and disadvantages of MOFs under different doping modifications, as well as the relationship between structure and catalytic conversion properties.

5. Conclusions and Perspectives

In recent years, doped materials have made significant progress in inhibiting the shuttle effect by enhancing their interaction with polysulfides through adjustments to their electronic structure and surface properties. This advancement has improved the practicality and reliability of lithium-sulfur batteries. In lithium-sulfur batteries, the slow conversion between soluble and insoluble $\text{Li}_2\text{S}_2/\text{Li}_2\text{S}$ is the main cause of the “shuttle effect” of LiPSs in the liquid electrolyte, which severely reduces the energy efficiency and cycling performance of the battery. Therefore, the ideal sulfur host should not only have a strong affinity for LiPSs, but also promote the mutual conversion of LiPSs and $\text{Li}_2\text{S}_2/\text{Li}_2\text{S}$, which is considered to be a feasible strategy to inhibit the “shuttle effect” of LiPSs.^[164] MOFs, as porous materials with high surface area and tunable pore size, have shown great potential for wide application in lithium-sulfur batteries. Firstly, MOFs can serve as carrier materials for sulfur cathodes, effectively preventing the expansion and contraction of sulfur during cycling. The highly ordered pore structure of MOFs can provide sufficient space to accommodate sulfur, avoiding sulfur overflow and depletion. Additionally, MOFs can be surface-functionalized to enhance the contact area between sulfur cathodes and electrolytes, thereby improving the rate and efficiency of electrochemical reactions. Secondly, MOFs can also be used as electrolyte additives to enhance the polarity performance of electrolytes, improving the battery’s cycle life and stability. With its abundant functional groups, MOFs can undergo ion exchange and surface adsorption with lithium ions, sulfur atoms, etc. in the electrolyte, forming stable ion transport channels to reduce electrode polarization and electrolyte decomposition, extending lifespan of the battery. Furthermore, MOFs can serve as conductive additives in electrode materials to enhance the conductivity and stability of electrodes. With excellent conductivity and high surface area, MOFs can effectively improve the conductivity of electrode materials, reduce electrode polarization, and enhance the charge transfer efficiency between electrodes and electrolytes, thereby improving LSB cycle life and energy density.

This study mainly focuses on the strategy of selective ligand doping to construct a series of MOF-based catalytic materials with excellent LiPSs adsorption and catalytic activity. Non-metal

Table 3. Summary of MOF structures and polysulfide catalytic mechanisms under different doping methods.

Doping methods	Structure	Cathode/Separator	Catalytic mechanisms	Advantages/disadvantages	Ref.
Non-metal doping	Construct a conductive network structure in conjunction with carbon cloth (CC@UiO-66(SH) ₂)	Separator	The thiol group binds to polysulfides through lithium bonds and covalent interactions for the chemical capture of polysulfides	Non-metal doping (such as nitrogen, sulfur, phosphorus, etc.) can enhance the chemical stability of MOFs and reduce polysulfide dissolution. Non-metal doping can also improve the conductivity of MOFs by introducing charge transfer or forming electronic conductors, and increase the number of new functional sites/The catalytic activity of non-metal doped MOFs is often lower, and the synthesis process may be more complex, requiring precise control of doping concentration and location, which could also affect the structural stability of the MOFs	[75]
	The CC moiety is coated on the surface of the MOF via C–N bonds (MOF@CC)	Separator	The C–N bonds at the MOF–carbon interface act as catalytic sites to accelerate the de-solvation of lithium ions and the conversion of polysulfides		[81]
	Sulfur immobilization in nitrogen-doped carbon derived from MOF	Cathode	Carbonization of nitrogen-containing MOF with abundant micropores and mesopores can effectively inhibit shuttle effects and alleviate volume expansion		[87]
	Nitrogen and sulfur co-doped hollow porous carbon shells derived from MOFs, embedded with g-C ₃ N ₄ (CN@NSHPS)	Cathode	The hollow design of the carbon shell, co-doping strategy, and embedding of g-C ₃ N ₄ synergistically promote the conversion of polysulfides		[90]
	Layer-by-layer N and P co-doped MOF-derived carbon material (MC–CN–CNP)	Separator	Sequential doping of nitrogen and phosphorus altered the electron cloud density of carbon atoms between different layers, thereby creating an internal electric field that enhances the redox kinetics		[94]
	Polyhedral structures derived from oxygen-containing MOFs with surfaces rich in carboxyl and hydroxyl functional groups (OMNC)	Separator	Microporous structures and graphene layers can provide three-dimensional electronic transport channels, while carboxyl and hydroxyl functional groups can synergistically enhance the physical and chemical effects for effective adsorption of sulfides		[112]
Single metal doping	Cobalt-based MOF carbonized into porous polyhedral carbon materials (Co–N–GC)	Cathode	The carbon network after carbonization can effectively capture polysulfides and forms Co–N pairs, which exhibit a dual catalytic effect on the polysulfide redox reactions	Single-metal doped MOFs (such as zinc, cobalt, iron, etc.) can provide additional catalytic sites, effectively promoting the conversion of polysulfides. Certain metal-doped MOFs (such as cobalt-doped MOFs) can significantly enhance the material's conductivity and, through metal doping, adjust the electronic environment and chemical properties of the MOFs, which helps optimize interactions with polysulfides and improve battery capacity and stability/Some single-metal doped MOFs may experience metal center dissolution or structural degradation during long-term cycling, and the synthesis cost may be higher, especially when using precious metals, which could limit their large-scale application	[115]
	Polyhedral porous structure (CrP@MOF)	Cathode	The rich catalytic adsorption sites on the Cr-based MOF surface can suppress the shuttle effect and accelerate the LiPS catalytic conversion		[117]
	The Ti-based MOF has a three-dimensional open framework structure with rich and uniform micropores (MIL-125(Ti))	Separator	The micropores in the framework ensure rapid transport of Li ⁺ ions and promote uniform lithium plating/stripping, while the O atoms of the BDC ligands in the Ti-based MOF exhibit strong affinity with Li ₂ S ₆ to suppress the shuttle effect		[120]
	MOF-808-M is composed of metal nodes and organic linkers, featuring a three-dimensional open porous structure	Cathode	The M-N ₂ O ₂ sites in MOF-808-M exhibit strong affinity for LiPSs; during the liquid-solid conversion process, the increase in free energy of MOF-808-M significantly promotes electrocatalysis		[126]
	Combining the framework stability of UiO-66 with the amino-functionalized framework structure (Ce–UiO-66-NH ₂)	Separator	The Ce ⁴⁺ metal sites exhibit Lewis acid properties, allowing strong interactions with LiPSs. The introduction of amino functionalization enhances the catalytic activity and selectivity for LiPSs		[129]
Bimetallic doping	A porous nitrogen-doped carbon substrate uniformly embedded with ZnPd alloy particles (ZnPd/NCF)	Separator	Lithium-affinitive Zn and sulfur-affinitive Pd can effectively catalyze the conversion reactions of lithium polysulfides, while the nitrogen-doped carbon substrate provides abundant	Bimetallic doping can optimize the electronic structure and catalytic sites of MOFs, leveraging the synergistic effects of two metals to improve the conversion reactions of polysulfides	[143]

Table 3. continued

Doping methods	Structure	Cathode/Separator	Catalytic mechanisms	Advantages/disadvantages	Ref.
The bimetallic Al/Cu-MOF exhibits a tetrahedral structure	Cathode	active sites that can effectively reduce self-discharge	The strong sulfur affinity of Cu ²⁺ effectively catalyzes the redox reactions of LiPSs, while the presence of Cu ²⁺ and Al ³⁺ provides abundant sites that enhance the adsorption capability for LiPSs	and enhance catalytic performance. Additionally, while maintaining high catalytic activity, it often also improves the stability of the material and reduces the loss of metal centers. The synthesis process of bimetallic doped MOFs is typically complex, requiring precise control over the ratio and distribution of the two metals. Additionally, interactions between the two metals may lead to unstable catalytic sites or unwanted side reactions, affecting the overall performance	[144]
The porous carbon nanofiber substrate is embedded with Cu–Mo bimetallic nanoparticles, exhibiting a three-dimensional porous structure	Cathode	Nitrogen doping can enhance the electronic conductivity of carbon fibers and provide additional catalytic sites; Cu can form chemical bonds with S, and Mo's tunable structure and variable oxidation states make the bimetallic synergistic effect an efficient catalyst for LiPS			[149]
The MOF shell grows on the surface of the sulfur species, integrating into a core-shell structure	Cathode	The MOF shell provides abundant catalytic sites, and the bimetals in the MOF bond with sulfur, synergistically facilitating the catalysis of polysulfides			[154]
The 3D Fe-ZIF-8 exhibits a nano-sheet flower structure.	Separator	The specific structure of the Fe-ZIF-8 modified separator promotes the catalytic conversion of soluble polysulfides into a solid form, and the presence of surface catalytic active metals facilitates the chemical reaction of polysulfides			[156]
MIL-101 (Cr) is a type of large-pore three-dimensional network structure with a pyramidal shape	Cathode	The synergistic effect between chromium and manganese oxides can enhance catalytic activity due to electron migration			[157]
The ultra-thin Ni–Co MOFs with unsaturated metal sites and conductive Ti ₃ C ₂ T _x nanosheets form a 2D/2D heterostructure.	Separator	Ti ₃ C ₂ T _x nanosheets, as a conductive substrate, provide electrons to Ni–Co MOFs and activate the unsaturated metal sites for the catalysis and conversion of LiPSs, achieving a synergistic adsorption-electrocatalysis effect on LiPSs.			[163]

doping can enhance the conductivity of MOFs, promote the diffusion of sulfur/lithium ions, reduce electrode polarization and sulfur shuttle, thereby improving the battery cycle life and energy density. Single metal doping can enhance catalytic activity, accelerate the reaction kinetics of sulfur, and improve the rate performance and cycling stability of the battery. Bimetallic doping can create an optimized metal coordination environment, promote sulfur atom adsorption and reduction, and enhance the rate performance and cycling life of the battery. In summary, non-metal, mono-metal, and bimetal doping of MOFs play important roles in improving the electrochemical performance, enhancing cycling stability, and increasing energy density of lithium-sulfur batteries, providing valuable insights for the development and application of lithium-sulfur batteries.

Although great progress has been made in the past few years, the application of the original MOF in batteries is still in its infancy, and more efforts should be made in the future. First,

due to the inherently poor electrical conductivity of most MOFs, which severely limits the rapid movement of electrons, there are additional considerations regarding their long-term electrochemical stability under repeated redox reactions. Moreover, doped metal or non-metal elements might react with the electrolyte in practical applications, potentially reducing stability and performance. To achieve more stable battery performance, we need to address the following issues: 1) Rational design of MOF structural configurations, future research can focus on developing new types of MOF materials. Compatible ligands and functional groups can introduce diversity in the framework, enhancing both physical and chemical functionalities. Combining conductive polymers or nanoconductive materials might be an effective approach to improving the conductivity of MOFs; 2) Optimization of doping strategies: in-depth exploration of doping strategies, especially optimizing dual-metal doping, could enhance the catalytic performance and stability of MOFs. Studying the synergistic effects of

different metals and the impact of doped elements on MOF structure and performance is an important direction for future research; 3) Particle size and morphology should be fully optimized. Such as, novel 2D MOF nanosheets can provide more active sites and shorten the diffusion pathways of ions/electrons; and 4) Comprehensive performance evaluation: establish a thorough performance evaluation system that not only focuses on the catalytic performance of the materials but also considers their long-term stability, economic viability, and environmental friendliness under practical usage conditions. In this review, MOF doping with heteroatoms to inhibit the shuttle effect of polysulfides and accelerate the kinetics of redox reactions is greatly explored, which greatly explores advanced lithium-sulfur batteries with high sulfur utilization, high energy density and long cycle life, and will further promote the electrochemical performance and practical application of Li-S batteries.

Conflict of Interests

The authors declare no conflict of interest.

Keywords: Lithium sulfur battery · MOF · Catalytic conversion · Shuttle effect

- [1] S. Han, P. Wen, H. Wang, Y. Zhou, Y. Gu, L. Zhang, Y. Shao-Horn, X. Lin, M. Chen, *Nat. Mater.* **2023**, *22*, 1515–1522.
- [2] Z. Wang, Z. Du, Y. Liu, C. E. Knapp, Y. Dai, J. Li, W. Zhang, R. Chen, F. Guo, W. Zong, X. Gao, J. Zhu, C. Wei, G. He, *eScience* **2023**, 100189.
- [3] A. Manthiram, *Nat. Commun.* **2020**, *11*, 1550.
- [4] J. Kersey, N. D. Popovich, A. A. Phadke, *Nat. Energy* **2022**, *7*, 664–674.
- [5] C. Xu, P. Behrens, P. Gasper, K. Smith, M. Hu, A. Tukker, B. Steubing, *Nat. Commun.* **2023**, *14*, 119.
- [6] C. Bauer, S. Burkhardt, N. P. Dasgupta, L. A.-W. Ellingsen, L. L. Gaines, H. Hao, R. Hischier, L. Hu, Y. Huang, J. Janek, C. Liang, H. Li, J. Li, Y. Li, Y.-C. Lu, W. Luo, L. F. Nazar, E. A. Olivetti, J. F. Peters, J. L. M. Rupp, M. Weil, J. F. Whitacre, S. Xu, *Nat. Sustainability* **2022**, *5*, 176–178.
- [7] J. Xiao, F. Shi, T. Glossmann, C. Burnett, Z. Liu, *Nat. Energy* **2023**, *8*, 329–339.
- [8] S. Huang, Z. Wu, B. Johannessen, K. Long, P. Qing, P. He, X. Ji, W. Wei, Y. Chen, L. Chen, *Nat. Commun.* **2023**, *14*, 5678.
- [9] K. Long, S. Huang, H. Wang, A. Wang, Y. Chen, Z. Liu, Y. Zhang, Z. Wu, W. Wang, L. Chen, *Energy Environ. Sci.* **2024**, *17*, 260–273.
- [10] P. Qing, Z. Wu, A. Wang, S. Huang, K. Long, T. Naren, D. Chen, P. He, H. Huang, Y. Chen, L. Mei, L. Chen, *Adv. Mater.* **2023**, *35*, 2211203.
- [11] W. Chen, Y. Hu, Y. Liu, S. Wang, A. Hu, T. Lei, Y. Li, P. Li, D. Chen, L. Xia, L. Xue, Y. Yan, G. Lu, M. Zhou, Y. Fan, H. Yang, X. Tao, X. Wang, Y. Li, J. Xiong, *Adv. Mater.* **2024**, *36*, 2312880.
- [12] S. Li, J. Huang, Y. Cui, S. Liu, Z. Chen, W. Huang, C. Li, R. Liu, R. Fu, D. Wu, *Nat. Nanotechnol.* **2022**, *17*, 613–621.
- [13] F. Liu, R. Xu, Y. Wu, D. T. Boyle, A. Yang, J. Xu, Y. Zhu, Y. Ye, Z. Yu, Z. Zhang, X. Xiao, W. Huang, H. Wang, H. Chen, Y. Cui, *Nature* **2021**, *600*, 659–663.
- [14] J. Wang, L. Wang, Z. Li, J. Bi, Q. Shi, H. Song, *J. Electron. Mater.* **2023**, *52*, 3526–3548.
- [15] J. Liu, Y. Zhou, T. Yan, X.-P. Gao, *Adv. Funct. Mater.* **2024**, *34*, 2309625.
- [16] Y. Huang, L. Lin, C. Zhang, L. Liu, Y. Li, Z. Qiao, J. Lin, Q. Wei, L. Wang, Q. Xie, D.-L. Peng, *Adv. Sci. (Weinh)* **2022**, *9*, 2106004.
- [17] M. A. Weret, C.-F. Jeffrey Kuo, T. S. Zeleke, T. T. Beyene, M.-C. Tsai, C.-J. Huang, G. B. Berhe, W.-N. Su, B.-J. Hwang, *Energy Storage Mater.* **2020**, *26*, 483–493.
- [18] W.-P. Wang, J. Zhang, J. Chou, Y.-X. Yin, Y. You, S. Xin, Y.-G. Guo, *Adv. Energy Mater.* **2021**, *11*, 2000791.
- [19] J. Wang, G. Li, D. Luo, Y. Zhang, Y. Zhao, G. Zhou, L. Shui, X. Wang, Z. Chen, *Adv. Energy Mater.* **2020**, *10*, 2002076.
- [20] A. Hagopian, M.-L. Doublet, J.-S. Filhol, *Energy Environ. Sci.* **2020**, *13*, 5186–5197.
- [21] Y. Zhou, X. Zhang, Y. Ding, J. Bae, X. Guo, Y. Zhao, G. Yu, *Adv. Mater.* **2020**, *32*, 2003920.
- [22] Q. Cheng, L. Wei, Z. Liu, N. Ni, Z. Sang, B. Zhu, W. Xu, M. Chen, Y. Miao, L.-Q. Chen, W. Min, Y. Yang, *Nat. Commun.* **2018**, *9*, 2942.
- [23] W. Deng, J. Phung, G. Li, X. Wang, *Nano Energy* **2021**, *82*, 105761.
- [24] W. Ren, Y. Zheng, Z. Cui, Y. Tao, B. Li, W. Wang, *Energy Storage Mater.* **2021**, *35*, 157–168.
- [25] D. Zheng, G. Wang, D. Liu, J. Si, T. Ding, D. Qu, X. Yang, D. Qu, *Adv. Mater. Technol.* **2018**, *3*, 1700233.
- [26] Y. Hu, W. Chen, T. Lei, Y. Jiao, J. Huang, A. Hu, C. Gong, C. Yan, X. Wang, J. Xiong, *Adv. Energy Mater.* **2020**, *10*, 2000082.
- [27] T. Li, X. Bai, U. Gulzar, Y.-J. Bai, C. Capiglia, W. Deng, X. Zhou, Z. Liu, Z. Feng, R. Proietti Zaccaria, *Adv. Funct. Mater.* **2019**, *29*, 1901730.
- [28] Q. Qi, X. Lv, W. Lv, Q.-H. Yang, *J. Energy Chem.* **2019**, *39*, 88–100.
- [29] M. Rana, S. A. Ahad, M. Li, B. Luo, L. Wang, I. Gentle, R. Knibbe, *Energy Storage Mater.* **2019**, *18*, 289–310.
- [30] Z. Shi, Y. Ding, Q. Zhang, J. Sun, *Adv. Energy Mater.* **2022**, *12*, 2201056.
- [31] G. Sui, J. Jun, L. Yang, Q. Rong, W. Zhao-yin, *Energy Storage Sci. Technol.* **2017**, *6*, 1026.
- [32] A. Wang, J. Li, T. Zhang, *Nat. Chem. Rev.* **2018**, *2*, 65–81.
- [33] Y. Xiao, Y. Xiang, S. Guo, J. Wang, Y. Ouyang, D. Li, Q. Zeng, W. Gong, L. Gan, Q. Zhang, S. Huang, *Energy Storage Mater.* **2022**, *51*, 882–889.
- [34] M. Rivera-Torreto, L. D. B. Mandemaker, M. Filez, G. Delen, B. Seoane, F. Meirer, B. M. Weckhuysen, *Chem. Soc. Rev.* **2020**, *49*, 6694–6732.
- [35] Q. Wang, R. Zou, W. Xia, J. Ma, B. Qiu, A. Mahmood, R. Zhao, Y. Yang, D. Xia, Q. Xu, *Small* **2015**, *11*, 2511–2517.
- [36] K. Khaletskaya, J. Reboul, M. Meiliikhov, M. Nakahama, S. Diring, M. Tsujimoto, S. Isoda, F. Kim, K.-i. Kamei, R. A. Fischer, S. Kitagawa, S. Furukawa, *J. Am. Chem. Soc.* **2013**, *135*, 10998–11005.
- [37] H. R. Moon, D.-W. Lim, M. P. Suh, *Chem. Soc. Rev.* **2013**, *42*, 1807–1824.
- [38] S. Horike, D. Umeyama, S. Kitagawa, *Acc. Chem. Res.* **2013**, *46*, 2376–2384.
- [39] R. Ricco, L. Malfatti, M. Takahashi, A. J. Hill, P. Falcaro, *J. Mater. Chem. A* **2013**, *1*, 13033–13045.
- [40] M.-S. Yao, W.-X. Tang, G.-E. Wang, B. Nath, G. Xu, *Adv. Mater.* **2016**, *28*, 5229–5234.
- [41] Y. Hu, J. Liu, C. Lee, M. Li, B. Han, T. Wu, H. Pan, D. Geng, Q. Yan, *Small* **2023**, *19*, 2300916.
- [42] G. Xia, J. Ye, Z. Zheng, X. Li, C. Chen, C. Hu, *Carbon* **2021**, *172*, 96–105.
- [43] J. Yang, S. Li, G. Wu, J. Bao, S. Xu, C. Gu, J. Lv, J. Huang, S. W. Joo, *J. Alloys Compd.* **2024**, *981*, 173701.
- [44] J. Qian, B. Jin, Y. Li, X. Zhan, Y. Hou, Q. Zhang, *J. Energy Chem.* **2021**, *56*, 420–437.
- [45] Y.-J. Yen, S.-H. Chung, *J. Mater. Chem. A* **2023**, *11*, 4519–4526.
- [46] X. Jing, Z. Hu, J. Qin, X. Jiang, M. Wang, S. Huo, S. Zhang, J. Wang, Y. Zhang, *J. Membr. Sci.* **2023**, *688*, 122118.
- [47] H. J. Kim, N. Umirov, J.-S. Park, J.-H. Lim, J. Zhu, S.-S. Kim, S.-T. Myung, *Energy Storage Mater.* **2022**, *46*, 76–89.
- [48] T. Cao, X. Cheng, M. Wang, J. Lu, J. Niu, H. Liu, X. Liu, Y. Zhang, *ACS Appl. Mater. Interfaces* **2023**, *15*, 6666–6675.
- [49] H. Zhang, S. Feng, X. Li, X. Chen, L. Chen, J. Xiao, *Colloids Surf. A* **2023**, *669*, 131440.
- [50] F. Chu, M. Yu, H. Jiang, J. Mu, X. Li, *J. Colloid Interface Sci.* **2022**, *627*, 838–847.
- [51] Z. Song, W. Jiang, B. Li, Y. Qu, R. Mao, X. Jian, F. Hu, *Small* **2024**, *20*, 2308550.
- [52] Q. Liang, S. Wang, Y. Yao, P. Dong, H. Song, *Adv. Funct. Mater.* **2023**, *33*, 2300825.
- [53] H. Jiang, J. Guo, J. Tao, X. Li, W. Zheng, G. He, Y. Dai, *ACS Appl. Energ. Mater.* **2022**, *5*, 2308–2317.
- [54] J. Long, H. Zhang, J. Ren, J. Li, M. Zhu, T. Han, B. Sun, S. Zhu, H. Zhang, J. Liu, *Electrochim. Acta* **2020**, *356*, 136853.
- [55] X. Ji, L. F. Nazar, *J. Mater. Chem.* **2010**, *20*, 9821–9826.
- [56] B. L. Ellis, K. T. Lee, L. F. Nazar, *Chem. Mater.* **2010**, *22*, 691–714.
- [57] M. Cuisinier, P.-E. Cabelguen, S. Evers, G. He, M. Kolbeck, A. Garsuch, T. Bolin, M. Balasubramanian, L. F. Nazar, *J. Phys. Chem. Lett.* **2013**, *4*, 3227–3232.
- [58] Y. Diao, K. Xie, S. Xiong, X. Hong, *J. Electrochem. Soc.* **2012**, *159*, A421.
- [59] L. Peng, Z. Wei, C. Wan, J. Li, Z. Chen, D. Zhu, D. Baumann, H. Liu, C. S. Allen, X. Xu, A. I. Kirkland, I. Shakir, Z. Almutairi, S. Tolbert, B. Dunn, Y. Huang, P. Sautet, X. Duan, *Nat. Catal.* **2020**, *3*, 762–770.
- [60] L. Zhou, D. L. Danilov, F. Qiao, J. Wang, H. Li, R.-A. Eichel, P. H. L. Notten, *Adv. Energy Mater.* **2022**, *12*, 2202094.

- [61] C. Yuan, X. Yang, P. Zeng, J. Mao, K. Dai, L. Zhang, X. Sun, *Nano Energy* **2021**, *84*, 105928.
- [62] X. Hu, T. Huang, G. Zhang, S. Lin, R. Chen, L.-H. Chung, J. He, *Coord. Chem. Rev.* **2023**, *475*, 214879.
- [63] T. Islamoglu, S. Goswami, Z. Li, A. J. Howarth, O. K. Farha, J. T. Hupp, *Acc. Chem. Res.* **2017**, *50*, 805–813.
- [64] H. Lu, Q. Zeng, L. Xu, Y. Xiao, L. Xie, J. Yang, J. Rong, J. Weng, C. Zheng, Q. Zhang, S. Huang, *Angew. Chem. Int. Ed.* **2024**, *63*, e202318859.
- [65] C. Li, H. Zhang, M. Liu, F.-F. Lang, J. Pang, X.-H. Bu, *Ind. Chem. Mater.* **2023**, *1*, 9–38.
- [66] C. Li, X. Zhang, Q. Zhang, Y. Xiao, Y. Fu, H. H. Tan, J. Liu, Y. Wu, *Comput. Theor. Chem.* **2021**, *1196*, 113110.
- [67] C.-L. Song, Z.-H. Li, L.-Y. Ma, M.-Z. Li, S. Huang, X.-J. Hong, Y.-P. Cai, Y.-Q. Lan, *ACS Nano* **2021**, *15*, 13436–13443.
- [68] X. Dong, X. Liu, P. K. Shen, J. Zhu, *Adv. Funct. Mater.* **2023**, *33*, 2210987.
- [69] Q. Deng, X. Dong, P. K. Shen, J. Zhu, *Adv. Sci. (Weinh)* **2023**, *10*, 2207470.
- [70] F. Liang, Q. Deng, S. Ning, H. He, N. Wang, Y. Zhu, J. Zhu, *Adv. Sci. (Weinh)* **2024**, *n/a*, 2403391.
- [71] T. Ren, X. Wang, N. Wang, D. Huang, Y. Zhu, P. K. Shen, J. Zhu, *J. Mater. Chem. A* **2024**, *12*, 5307–5318.
- [72] J. Li, Z. Niu, C. Guo, M. Li, W. Bao, *J. Energy Chem.* **2021**, *54*, 434–451.
- [73] Z. Tang, S. Zhou, Y. Huang, H. Wang, R. Zhang, Q. Wang, D. Sun, Y. Tang, H. Wang, *Electrochem. Energy Rev.* **2023**, *6*, 8.
- [74] L. Zhang, X. Chen, F. Wan, Z. Niu, Y. Wang, Q. Zhang, J. Chen, *ACS Nano* **2018**, *12*, 9578–9586.
- [75] X. Hu, S. Lin, R. Chen, G. Zhang, T. Huang, J. Li, X. Yang, L.-H. Chung, L. Yu, J. He, *ACS Appl. Mater. Interfaces* **2022**, *14*, 31942–31950.
- [76] S. Zheng, X. Zhao, G. Liu, F. Wu, J. Li, *Nanotechnology* **2021**, *32*, 365404.
- [77] J. Qian, W. A. Henderson, W. Xu, P. Bhattacharya, M. Engelhard, O. Borodin, J.-G. Zhang, *Nat. Commun.* **2015**, *6*, 6362.
- [78] Z. Wang, Y. Sun, Y. Mao, F. Zhang, L. Zheng, D. Fu, Y. Shen, J. Hu, H. Dong, J. Xu, X. Wu, *Energy Storage Mater.* **2020**, *30*, 228–237.
- [79] Y. Hu, L. Li, H. Tu, X. Yi, J. Wang, J. Xu, W. Gong, H. Lin, X. Wu, M. Liu, *Adv. Funct. Mater.* **2022**, *32*, 2203336.
- [80] Z. Yu, N. P. Balsara, O. Borodin, A. A. Gewirth, N. T. Hahn, E. J. Maginn, K. A. Persson, V. Srinivasan, M. F. Toney, K. Xu, K. R. Zavadil, L. A. Curtiss, L. Cheng, *ACS Energy Lett.* **2022**, *7*, 461–470.
- [81] L. Li, H. Tu, J. Wang, M. Wang, W. Li, X. Li, F. Ye, Q. Guan, F. Zhu, Y. Zhang, Y. Hu, C. Yan, H. Lin, M. Liu, *Adv. Funct. Mater.* **2023**, *33*, 2212499.
- [82] T. Yang, H. Zeng, W. Wang, X. Zhao, W. Fan, C. Wang, X. Zuo, R. Zeng, J. Nan, *J. Mater. Chem. A* **2019**, *7*, 8292–8301.
- [83] Y. S. Park, J. Yang, J. Lee, M. J. Jang, J. Jeong, W.-S. Choi, Y. Kim, Y. Yin, M. H. Seo, Z. Chen, S. M. Choi, *Appl. Catal. B* **2020**, *278*, 119276.
- [84] T.-Z. Hou, X. Chen, H.-J. Peng, J.-Q. Huang, B.-Q. Li, Q. Zhang, B. Li, *Small* **2016**, *12*, 3283–3291.
- [85] D. G. Xiong, Z. Zhang, X. Y. Huang, Y. Huang, J. Yu, J. X. Cai, Z. Y. Yang, *J. Energy Chem.* **2020**, *51*, 90–100.
- [86] S. Yuan, J. L. Bao, L. Wang, Y. Xia, D. G. Truhlar, Y. Wang, *Adv. Energy Mater.* **2016**, *6*, 1501733.
- [87] Z. Li, L. Yin, *ACS Appl. Mater. Interfaces* **2015**, *7*, 4029–4038.
- [88] S. Xin, L. Gu, N.-H. Zhao, Y.-X. Yin, L.-J. Zhou, Y.-G. Guo, L.-J. Wan, *J. Am. Chem. Soc.* **2012**, *134*, 18510–18513.
- [89] J. Gao, M. A. Lowe, Y. Kiya, H. D. Abruña, *J. Phys. Chem. C* **2011**, *115*, 25132–25137.
- [90] H. Zhang, Z. Zhao, Y.-N. Hou, Y. Tang, Y. Dong, S. Wang, X. Hu, Z. Zhang, X. Wang, J. Qiu, *J. Mater. Chem. A* **2018**, *6*, 7133–7141.
- [91] X. Fang, Y. Jiang, K. Zhang, G. Hu, W. Hu, *New J. Chem.* **2021**, *45*, 2361–2365.
- [92] K. Chen, Z. Sun, R. Fang, Y. Shi, H.-M. Cheng, F. Li, *Adv. Funct. Mater.* **2018**, *28*, 1707592.
- [93] L. Ji, Y. Jia, X. Wang, L. Duan, W. Li, J. Liu, Y. Zhang, *Nanotechnology* **2021**, *32*, 192002.
- [94] G. Sun, T. Yang, J. Duan, Y. Zhang, M. Wang, R. Wang, C. Wang, *J. Alloys Compd.* **2021**, *870*, 159543.
- [95] K. Lu, Z. Hu, J. Ma, H. Ma, L. Dai, J. Zhang, *Nat. Commun.* **2017**, *8*, 527.
- [96] C. Li, Z. Xi, D. Guo, X. Chen, L. Yin, *Small* **2018**, *14*, 1701986.
- [97] J. Wang, W.-Q. Han, *Adv. Funct. Mater.* **2022**, *32*, 2107166.
- [98] J. Meng, C. Niu, L. Xu, J. Li, X. Liu, X. Wang, Y. Wu, X. Xu, W. Chen, Q. Li, Z. Zhu, D. Zhao, L. Mai, *J. Am. Chem. Soc.* **2017**, *139*, 8212–8221.
- [99] J. Tang, R. R. Salunkhe, H. Zhang, V. Malgras, T. Ahamed, S. M. Alshehri, N. Kobayashi, S. Tominaka, Y. Ide, J. H. Kim, Y. Yamauchi, *Sci. Rep.* **2016**, *6*, 30295.
- [100] H. Jin, H. Zhou, W. Li, Z. Wang, J. Yang, Y. Xiong, D. He, L. Chen, S. Mu, *J. Mater. Chem. A* **2018**, *6*, 20093–20099.
- [101] X. X. Wang, D. A. Cullen, Y.-T. Pan, S. Hwang, M. Wang, Z. Feng, J. Wang, M. H. Engelhard, H. Zhang, Y. He, Y. Shao, D. Su, K. L. More, J. S. Spendel, G. Wu, *Adv. Mater.* **2018**, *30*, 1706758.
- [102] N. Zafar, S. Yun, M. Sun, J. Shi, A. Arshad, Y. Zhang, Z. Wu, *ACS Catal.* **2021**, *11*, 13680–13695.
- [103] H. Li, Y. Su, W. Sun, Y. Wang, *Adv. Funct. Mater.* **2016**, *26*, 8345–8353.
- [104] J. Balamurugan, A. Pandurangan, N. H. Kim, J. H. Lee, *Nanoscale* **2015**, *7*, 679–689.
- [105] F. Han, S. Yun, J. Shi, Y. Zhang, Y. Si, C. Wang, N. Zafar, J. Li, X. Qiao, *Appl. Catal. B* **2020**, *273*, 119004.
- [106] A. Patra, J. E. Bates, J. Sun, J. P. Perdew, *Proc. Nat. Acad. Sci.* **2017**, *114*, E9188–E9196.
- [107] X. Liu, Z. Liu, W. Yang, M. Wang, B. Qin, Y. Zhang, Z. Liu, H. Fan, *Mater. Today Chem.* **2022**, *26*, 101002.
- [108] C. Yao, J. Xu, Y. Zhu, R. Zhang, Y. Shen, A. Xie, *Appl. Surf. Sci.* **2020**, *513*, 145777.
- [109] X. Ma, C. Ji, X. Yu, Y. Liu, X. Xiong, *ACS Appl. Mater. Interfaces* **2021**, *13*, 53965–53973.
- [110] J. Lin, K. Zhang, Z. Zhu, R. Zhang, N. Li, C. Zhao, *ACS Appl. Mater. Interfaces* **2020**, *12*, 2497–2504.
- [111] H. Zhu, S. Dong, J. Xiong, P. Wan, X. Jin, S. Lu, Y. Zhang, H. Fan, *J. Colloid Interface Sci.* **2023**, *641*, 942–949.
- [112] W. Li, Y. Ye, J. Qian, Y. Xing, W. Qu, N. Zhang, L. Li, F. Wu, R. Chen, *ChemElectroChem* **2019**, *6*, 1094–1100.
- [113] F. Zheng, Y. Yang, Q. Chen, *Nat. Commun.* **2014**, *5*, 5261.
- [114] H. Al Salem, G. Babu, C. V. Rao, L. M. R. Arava, *J. Am. Chem. Soc.* **2015**, *137*, 11542–11545.
- [115] Y.-J. Li, J.-M. Fan, M.-S. Zheng, Q.-F. Dong, *Energy Environ. Sci.* **2016**, *9*, 1998–2004.
- [116] Z. Li, C. Li, X. Ge, J. Ma, Z. Zhang, Q. Li, C. Wang, L. Yin, *Nano Energy* **2016**, *23*, 15–26.
- [117] X. Zhang, Z. Shen, Y. Wen, Q. He, J. Yao, H. Cheng, T. Gao, X. Wang, H. Zhang, H. Jiao, *ACS Appl. Mater. Interfaces* **2023**, *15*, 21040–21048.
- [118] C. Zhou, M. Chen, C. Dong, H. Wang, C. Shen, X. Wu, Q. An, G. Chang, X. Xu, L. Mai, *Nano Energy* **2022**, *98*, 107332.
- [119] Z. Ye, Y. Jiang, L. Li, F. Wu, R. Chen, *Adv. Mater.* **2020**, *32*, 2002168.
- [120] C. Qi, L. Xu, J. Wang, H. Li, C. Zhao, L. Wang, T. Liu, *ACS Sustainable Chem. Eng.* **2020**, *8*, 12968–12975.
- [121] M. Rana, M. Li, X. Huang, B. Luo, I. Gentle, R. Knibbe, *J. Mater. Chem. A* **2019**, *7*, 6596–6615.
- [122] D.-D. Han, Z.-Y. Wang, G.-L. Pan, X.-P. Gao, *ACS Appl. Mater. Interfaces* **2019**, *11*, 18427–18435.
- [123] Q. Pang, X. Liang, C. Y. Kwok, L. F. Nazar, *J. Electrochem. Soc.* **2015**, *162*, A2567.
- [124] J. Zheng, J. Tian, D. Wu, M. Gu, W. Xu, C. Wang, F. Gao, M. H. Engelhard, J.-G. Zhang, J. Liu, J. Xiao, *Nano Lett.* **2014**, *14*, 2345–2352.
- [125] X. Liang, A. Garsuch, L. F. Nazar, *Angew. Chem.* **2015**, *127*, 3979–3983.
- [126] S. He, J. Yang, S. Liu, X. Wang, J. Qiu, *Adv. Funct. Mater.* **2023**, *n/a*, 2314133.
- [127] X.-J. Hong, C.-L. Song, Y. Yang, H.-C. Tan, G.-H. Li, Y.-P. Cai, H. Wang, *ACS Nano* **2019**, *13*, 1923–1931.
- [128] M. Zhou, Y. Li, T. Lei, W. Chen, G. Rao, L. Xue, A. Hu, Y. Fan, J. Huang, Y. Hu, X. Wang, J. Xiong, *Small* **2021**, *17*, 2104367.
- [129] Y. Su, W. Wang, W. Wang, A. Wang, Y. Huang, Y. Guan, *J. Electrochem. Soc.* **2022**, *169*, 030528.
- [130] L. Ma, R. Chen, G. Zhu, Y. Hu, Y. Wang, T. Chen, J. Liu, Z. Jin, *ACS Nano* **2017**, *11*, 7274–7283.
- [131] L. Zhang, M. Ling, J. Feng, G. Liu, J. Guo, *Nano Energy* **2017**, *40*, 559–565.
- [132] Y. Chu, X. Cui, W. Kong, K. Du, L. Zhen, L. Wang, *Chem. Eng. J.* **2022**, *427*, 130844.
- [133] X. Wang, Y. Wang, F. Wu, G. Jin, J. Li, Z. Zhang, *Appl. Surf. Sci.* **2022**, *596*, 153628.
- [134] R. Tian, S.-H. Park, P. J. King, G. Cunningham, J. Coelho, V. Nicolosi, J. N. Coleman, *Nat. Commun.* **2019**, *10*, 1933.
- [135] X. Zhou, T. Liu, G. Zhao, X. Yang, H. Guo, *Energy Storage Mater.* **2021**, *40*, 139–149.
- [136] D. Liu, C. Zhang, G. Zhou, W. Lv, G. Ling, L. Zhi, Q.-H. Yang, *Adv. Sci. (Weinh)* **2018**, *5*, 1700270.
- [137] C. Dong, C. Zhou, Y. Li, Y. Yu, T. Zhao, G. Zhang, X. Chen, K. Yan, L. Mai, X. Xu, *Small* **2023**, *19*, 2205855.
- [138] P. Zeng, X. Zhou, J. Peng, X. Huang, B. Chang, G. Chen, M. Chen, L. Zheng, Y. Pei, J. Su, X. Wang, *Adv. Funct. Mater.* **2023**, *33*, 2211818.

- [139] M. Zhang, W. Chen, L. Xue, Y. Jiao, T. Lei, J. Chu, J. Huang, C. Gong, C. Yan, Y. Yan, Y. Hu, X. Wang, J. Xiong, *Adv. Energy Mater.* **2020**, *10*, 1903008.
- [140] J. Zhang, J. Yang, Z. Liu, B. Zheng, *ACS Omega* **2021**, *6*, 4995–5000.
- [141] V. P. Nguyen, J.-H. Kim, S.-M. Lee, *Mater. Today Energy* **2023**, *38*, 101451.
- [142] S. Deng, T. Guo, J. Heier, C. Zhang, *Adv. Sci. (Weinh)* **2023**, *10*, 2204930.
- [143] H.-J. Zhou, X.-L. Zhang, M.-Y. Zou, S.-T. Gu, Y.-P. Cai, X.-J. Hong, *ACS Appl. Energ. Mater.* **2021**, *4*, 13183–13190.
- [144] P. Geng, M. Du, X. Guo, H. Pang, Z. Tian, P. Braunstein, Q. Xu, *Energy Environ. Mater.* **2022**, *5*, 599–607.
- [145] S. Bai, X. Liu, K. Zhu, S. Wu, H. Zhou, *Nat. Energy* **2016**, *1*, 16094.
- [146] R. Zhao, Z. Liang, S. Gao, C. Yang, B. Zhu, J. Zhao, C. Qu, R. Zou, Q. Xu, *Angew. Chem. Int. Ed.* **2019**, *58*, 1975–1979.
- [147] J. Wang, W. Liu, G. Luo, Z. Li, C. Zhao, H. Zhang, M. Zhu, Q. Xu, X. Wang, C. Zhao, Y. Qu, Z. Yang, T. Yao, Y. Li, Y. Lin, Y. Wu, Y. Li, *Energy Environ. Sci.* **2018**, *11*, 3375–3379.
- [148] B. He, Q. Zhang, P. Man, Z. Zhou, C. Li, Q. Li, L. Xie, X. Wang, H. Pang, Y. Yao, *Nano Energy* **2019**, *64*, 103935.
- [149] Z. Cheng, H. Pan, Z. Wu, M. Wübbenhörst, Z. Zhang, *ACS Appl. Mater. Interfaces* **2022**, *14*, 45688–45696.
- [150] L. Zeng, Y. Jiang, J. Xu, M. Wang, W. Li, Y. Yu, *Nanoscale* **2015**, *7*, 10940–10949.
- [151] X. Wang, J. Han, C. Luo, B. Zhang, J. Ma, Z. Li, Y.-B. He, Q.-H. Yang, F. Kang, W. Lv, *Small* **2021**, *17*, 2101538.
- [152] Z. Cheng, Y. Chen, Y. Yang, L. Zhang, H. Pan, X. Fan, S. Xiang, Z. Zhang, *Adv. Energy Mater.* **2021**, *11*, 2003718.
- [153] H. Dai, L. Wang, Y. Zhao, J. Xue, R. Zhou, C. Yu, J. An, J. Zhou, Q. Chen, G. Sun, W. Huang, *Research* **2021**.
- [154] X. Ren, Q. Wang, Y. Pu, Q. Sun, W. Sun, L. Lu, *Adv. Mater.* **2023**, *35*, 2304120.
- [155] H. Zhang, J. Chen, Z. Li, Y. Peng, J. Xu, Y. Wang, *Adv. Funct. Mater.* **2023**, *33*, 2304433.
- [156] R. Razaq, M. M. U. Din, D. R. Småbråten, V. Eyupoglu, S. Janakiram, T. O. Sunde, N. Allahgoli, D. Rettenwander, L. Deng, *Adv. Energy Mater.* **2024**, *14*, 2302897.
- [157] S. Chen, Z. Zhang, J. Wang, P. Dong, *Materials (Basel)* **2023**.
- [158] C. Serre, F. Millange, C. Thouvenot, M. Noguès, G. Marsolier, D. Louér, G. Férey, *J. Am. Chem. Soc.* **2002**, *124*, 13519–13526.
- [159] G. Férey, C. Mellot-Draznieks, C. Serre, F. Millange, J. Dutour, S. Surblé, I. Margiolaki, *Science* **2005**, *309*, 2040–2042.
- [160] X. Han, Z. Zhang, X. Xu, *J. Mater. Chem. A* **2021**, *9*, 12225–12235.
- [161] X. Han, T. Zhang, W. Chen, B. Dong, G. Meng, L. Zheng, C. Yang, X. Sun, Z. Zhuang, D. Wang, A. Han, J. Liu, *Adv. Energy Mater.* **2021**, *11*, 2002753.
- [162] H. Lu, X. Kong, H. Huang, Y. Zhou, Y. Chen, *J. Environ. Sci.* **2015**, *32*, 102–107.
- [163] Y. Ren, Q. Zhai, B. Wang, L. Hu, Y. Ma, Y. Dai, S. Tang, X. Meng, *Chem. Eng. J.* **2022**, *439*, 135535.
- [164] Y. Jin, N. Deng, Y. Li, H. Wang, M. Zhang, W. Kang, B. Cheng, *J. Energy Chem.* **2024**, *88*, 469–512.

Manuscript received: July 14, 2024

Revised manuscript received: August 22, 2024

Version of record online: November 13, 2024
